Modeling the Formation of the Hemozoin Crystal in the Presence of Antimalarials: A Theoretical Study

Cristian Alirio Parra

a dissertation
submitted to the University of Antioquia
in candidacy for the Masters Degree on Physics

Advisor: Olga Lucia Lopez Acevedo
Co-advisor: Sergio Cruz-León

Faculty of Exact and Natural Sciences
December 2023

Abstract

This thesis centers around the modeling of the malaria crystal hemozoin (HZ), formed in the interior of the parasites digestive vacuole. In particular, the interaction of the antimalarials artesunate and chloroquine with the synthetic analog of HZ, β-hematin (BH).

To answer this question, we worked with experimental data provided to us by our collaborators in the *Solid State, Residue Analysis and Malaria Research Groups, from the Faculty of Exact and Natural Sciences of the University of Antioquia* and fitted the kinetics of BH formation in an aqueous and aqueous-octanol solutions that mimic the interior environment of the parasites digestive vacuole DV (where the crystal forms) in the presence and absence of the aforementioned antimalarial under a 10 and 30 mg concentration of each, to 10 kinetics models of crystallization, but only working with the two most relevant ones for the reminder of this work. One proposed by Pasternack et al.[1]., and a second order model proposed by the collaboration[2]. Both models use the classical nucleation theory (CNT) description of the nucleation and growth process to represent the experimental data, but only our model proposes a term associated with the formation of the basic crystallization unit needed to form the crystal (a β-hematin dimer).

We proceeded to use the experimental IR data, also provided by the mentioned groups, to the BH crystal when zero and 30 mg of the antimalarial chloroquine is present in the solution that formed the studied crystals, and proceeded to simulate the IR spectra of the β-hematin dimer with ASE[3] and GPAW[4] codes, and compared the simulated and experimental peaks, analyzing the vibrations/trajectories generated by the simulations to known peaks to confirm the validity of the obtained results and proceeded to extrapolate to the variations observed on the experimental peaks between the no drug and the 30 mg case, suggesting that the differences observed correspond to the absence of methyl and vinyl group bonds attributed to the antimalarial.

This work finishes with a simple implementation of a nucleation and growth model under the CNT assumptions using a cellular automaton based on Conway's game of life automaton with modified neighbor rules to represent the seed formation process in the solution as we change the concentration of available solute and seeing how these changes affect the morphology of the generated seeds.

We hope that this theoretical work, can shed some light into possible yet simple avenues to explore the crystallization process that underlies the survival of the malaria parasite, aiding our understanding of its behavior and helping us develop new antimalarials, as the crystal is

a target of current ones, shielding vulnerable populations from the deadly and ever-evolving parasite.

Contents

Listing of figures

List of Tables

List of Abbreviations

HZ Hemozoin

BH β-Hematin

DV Digestive Vacuole

CQ Chloroquine

AT Artesunate

SOM Second Order Model

DFT Density Functional Theory

CA Cellular Automaton

This work is dedicated to my mentors, family, and friends.

Acknowledgments

I have been lucky enough to find along the way wise and kind people who have enriched me with their company and their brilliance. This can't be more true in the case of my advisors Olga and Sergio, both of them believed in me, giving me space to make mistakes and to reflect on them, followed by clear and honest advice. I thank them deeply for their openness and willingness to share their time and hard-earned knowledge that many times went beyond academia, not only helping me be a better scientist but a person overall. Interacting with them, I saw creative, hard-working people filled with passion and love for what they do, always ready to learn from others, I hope to carry these values with me wherever I go and honor their teachings with my work, thank you.

To my family for supporting me with their love, time, and efforts. While I have been pursuing my love of science, they have been there holding my back, encouraging me in the midst of difficult and hard moments. Without them and the love that they provided me, I would be lost in darkness, they represent the values that I admire the most and the ones that I always try to carry every day: unshakable will, honesty, dedication, integrity, kindness, patience, wisdom, and love.

To my friends who have been there for me, even in the times I couldn't be with them as much as I wanted. They have filled my life with joy and warmth, ready to support and confront me in equal parts, giving me perspective and clarity.

I would like to finish by saying that I have always strived to be of service to those whose path crossed with mine, and what I have found is that it has been all of them who have enriched me and guided me through it. My humble wish is to honor all the efforts and sacrifices made by these people who putted their faith in me and to say from the bottom of my heart, thank you for every thing.

0 Introduction

0.1 The Importance of Malaria Research

Malaria is a disease common in tropical and subtropical regions that affects half of the world population [5].

The disease is lethal, but treatment reduces the chance of becoming a severe and life-threatening, particularly in children under 5, pregnant women and immunocompromised individuals [6].

It is transmitted to humans by the bite of an infected mosquito carrying any of the four species of unicellular parasites from the genus *Plasmodium* (*Vivax, Ovale, Malariae, Knowlesi* and *Falciparum*). *Plasmodium falciparum* is responsible alone for at least 50% of all the malaria cases in humans and around 95% of the deaths associated with it,[7]. The World Health Organization (WHO) Malaria Report 2022 estimated 619,000 malaria deaths globally in 2021, half of which occurred in four African countries: Nigeria (31%), the Democratic Republic of the Congo (13%), Niger (4%) and the United Republic of Tanzania (4%)[6].

The current treatment for malaria is based on the antimalarial artemisinin. It was obtained around 1971 from the sweet wormwood plant, and thanks to its efficiency, by 1990 it became the standard treatment[8] known as artemisinin-based combination therapies, where artemisinin is used in tandem with other antimalarials. Nonetheless, In 2010, evidence of partial resistance to artemisinin-based antimalarials appeared in the Greater Mekong Subregion and Africa[9]. This is not the first time that the malaria parasite has evolved to withstand antimalarial treatments. Chloroquine is an antimalarial produced around 1930. It is the synthetic version of the molecule quinine (found in the bark of the cinchona tree)[10]. Extensively used due to its safety, efficacy, and cheap production costs[11]. But, due to its indiscriminate use, selective pressure on the parasite pushed it to evolve resistance to chloroquine around 1950–1960 in the Greater Mekong Subregion and Latin America[12,13]. As resistance became widespread, it rendered the drug less effective[14]. Chloroquine is still used to treat malaria as an auxiliary in artemisinin-combination therapies.

The conclusion is clear: we are at a pivotal moment as the most effective treatment up to date is being overtaken by the ever-evolving parasite. This means that it is crucial to continue to study the parasite and the current antimalarials, and develope new, effective, cheap and

safe antimalarials to combat the disease.

0.2 Towards an Understanding of Hemozoin Formation

The life cycle of the malaria parasite (*Plasmodium Falciparum*) involves two hosts, mosquitoes and humans, where it has to transmit and develop in both to complete its reproductive cicle. While the malaria parasite is harmless to mosquitoes, it is lethal to its human hosts. The symptoms associated with malaria in humans are the byproduct of the Red Blood Cell (RBC) consumption phase of the infection, also called erythrocytic cycle. In this stage, the parasite ingests hemoglobin into its Digestive Vacuole (DV), where hemoglobin is catabolized and used for energy[15], releasing free heme molecules ($Fe^{II}C_{34}H_{32}O_4N_4$) also called ferrous-protoporphyrin IX. Heme oxidizes to $Fe^{III}C_{34}H_{32}O_4N_4$ called ferric-protoporphyrin IX (Fe-PPIX)[16], that is toxic to cells due to the reactive iron[17] and capable of membrane rupture[18]. The parasite sequesters the newly released and oxidized heme molecules, dimerizing them by the reciprocal carboxylate group of each Fe-PPIX bonding to the central iron of its corresponding partner [$Fe^{III} - O - C(=O)CH_2CH_2$]. This forms the basic unit of the crystal, a cyclic centrosymmetric ferric-heme dimers also called μ-propionated. The dimers interlink to one another by hydrogen bonds between the extra free propionated groups of each dimer ($O - H \cdots O = C$) and stack together, forming sheets that overlap one on top of the other to form the crystal[19 20 21]. The final structure is an insoluble, nonreactive and non-toxic, triclinic crystal[1], known as the malaria pigment Hemozoin (HZ) with approximate dimensions of $100\,\text{nm} \times 100\,\text{nm} \times 500\,\text{nm}$[16].

The formation of the crystal is a heme detoxification mechanism for the parasite that is crucial to its survival. For this reason, it has been the target of antimalarials[22 23]. Neverthe-

less, the exact process used by the parasite to produce the biocrystallization of heme is not known. However, there is consensus that the underlying mechanism of biomineralization follows a classical nucleation and growth (CNT) process[24,25]. This means that the transition from free-heme in a solution to crystallized hemozoin inside the DV is mediated by the formation of small clusters (seeds) that exhibit the properties of the emerging phase (the crystal)[26]. Nonetheless, the impact of factors such as the chemical environment of the DV, the role of proteins or lipid mediation on the rate of crystal formation are not clear. Researchers have used the synthetic analog of HZ, called β-hematin (BH), to study the mechanisms of HZ formation, the medium for crystal growth and the modes of action of antimalarials[27]. In particular, trying to understand how the medium and the drugs affect the kinetics, morphology[28], and total yield of crystal formed.

In this work, we fitted the kinetics of BH formation in an aqueous and aqueous-octanol solution under different concentrations of the antimalarials artesunate ($\{C_{19}H_{28}O_8$) and chloroquine (CQ) ($C_{18}H_{26}ClN_3$). For this, we used the experimental data provided to us in collaboration with the *Solid State, Residue Analysis and Malaria Research Groups, from the Faculty of Exact and Natural Sciences of the University of Antioquia*. The experimental group synthesized the crystals in the aqueous medium by dissolving bovine hemin in a NAOH and distilled water solution that is stirred for 30 minutes. The temperature is raised and kept at 60 °C for 4 hours. At this moment, acetic acid is introduced in the solution forming an acetate buffer with a pH of 4.75, close to the pH of 5 present in the digestive vacuole of the parasite. For the aqueous-organic medium, hemin is dissolved in a NaOH solution, then dimethyl sulfoxide (DMSO) is added. The mixture is heated to 40 °C and stirred for 30 minutes. The temperature is increased to 60 °C and acetic acid is mixed alongside octanol

and stirred every 25 minutes for 3 hours. The antimalarials chloroquine and artesunate in both cases are introduced by mixing the 10 or 30 mg concentration in the NaOH solution where heme is dissolved.

The models used to make the fitting were proposed by: Pasternack et al., in the paper *"On the Kinetics of Formation of Hemozoin, the Malaria Pigment"*, where the crystallization is modeled by a simple exponential and an Avrami kinetic curve. And the other model was proposed in collaboration with the experimental group and our group [2], based on the tendency of heme to self-associate [29], using a second order kinetic, and the nucleation and growth process by a logistic curve. We analyzed the effect of the antimalarials previously mentioned under the gaze of the theoretical description that both models lend us, and the effective changes present in the fitted parameters.

Furthermore, we compared the simulated infrared spectrum (IR) of a BH dimer obtained by DFT methods [30] with the experimental IR spectrums of the BH crystal, obtained by our collaborators, with and without the antimalarial chloroquine present [31]. The trajectories obtained from the simulation were ascribed to vibrations in the experimental IR and compared with other references that had assigned them to specific molecular vibrations on the crystal [32] to understand the relation between the bonds in the crystal and the antimalarial.

Finally, as a proof of concept, we used a cellular automaton [33] to study qualitatively the process of nucleation and growth, using the concentration of heme in the solution as a free parameter to characterize the behavior of the nucleation seeds formed in this simulation.

0.3 Statement of the Problem

Hypotheses

- The process of BH formation and inhibition by antimalarials can be modeled by the kinetics of crystallization under the assumption of nucleation and growth.
- The interaction with the antimalarials changes either the nucleation or growth process, depending on the possible mode of action of the antimalarials.
- Given the tendency of heme to self-associate, we consider that the formation of μ-propionate dimers from self-associated $\pi-\pi$ dimers can be considered a rate-determining step in the kinetics of crystallization.
- By modeling the BH dimer and using DFT methods to calculate the IR spectra, we can provide atomistic insight by comparing with the experimental IR of BH formation in the absence and presence of antimalarials. By studying the trajectories of the dimer, we can relate them to possible interactions with the antimalarials.
- Given that a cellular automata is a model of computation, it is possible to model the process of nucleation and growth in it by considering the neighborhood and the rules between neighbors of the cell and capture part of the behavior present in BH formation

Objectives

General Objective

To model the process of nucleation and growth of the HZ/BH crystal in the absence and presence of antimalarials by fitting experimental kinetic data, a simulated IR spectra and a cellular automaton to represent the nucleation seeds. This is done to elucidate the possible modes of action of the antimalarials (heme capture, adsorption to the surface) and the influence of the medium in the crystal formation process.

Specific Objectives

- To develop a kinetic model in which the process of nucleation and growth are represented, and analyze the effect of the antimalarial in each component of the model as a tool to understand the possible role played by the antimalarials in the process of crystal formation.
- To simulate the IR spectra of the BH dimer and compare it with the experimental spectra of BH in the absence and presence of the antimalarial chloroquine to understand the possible impact that this antimalarial may have in the crystal formation. In particular, how the antimalarial binds to the surface or the faces of the crystal.
- To use a cellular automata model to represent the process of crystal nucleation and growth.

Por eso en todo pensamiento encontramos una voz singular

en busca de una razón común.

Marina Garcés

1

Kinetics of β-Hematin Formation in the Presence of Antimalarials

1.1 Introduction

In this chapter, we delve into the fitting of the kinetic curves of BH formation in two mediums, an aqueous and aqueous-lipid solution, in order to understand the crystallization pro-

cess in the presence and absence of the antimalarials artesunate ($C_{19}\,H_{28}\,O_8$) and chloroquine ($C_{18}\,H_{26}\,Cl\,N_3$). The experimental data needed to fit the theoretical models was provided to us in collaboration with the *Solid State, Residue Analysis and Malaria Research Groups, from the Faculty of Exact and Natural Sciences of the University of Antioquia* and with whom we explored the two models of crystallization that will be presented here, one proposed by Pasternack et al.,[1] and a second order kinetic process of crystallization developed by the collaborative effort of these groups and us[2].

We compared both theoretical models in different media, antimalarials, and concentration. Relating changes to the fittings to the modes of action of the antimalarials and the medium on the crystallization process. We start the chapter with the basic concepts of kinetic theory, crystal nucleation and growth and go on to apply them to the models and interpret it.

1.2 Basic Concepts on Kinetics and Crystallization

The subject of kinetics deals with the temporal relations between the concentrations of the reactants (ingredients needed for a reaction) and the products –the ingredients produced by the reaction–. Studying these relations contextualizes why some processes take place much faster than others, helping us understand how the reactants change into the products as the reaction takes place, also known as the pathway of the reaction, reaching chemical and thermodynamic equilibrium. By only considering the overall energy differences between the initial and final states of the reaction (thermodynamics), we glimpse into feasible and infeasible processes, but not the time needed for the processes to occur. Consider two containers with molecular hydrogen and oxygen. If a slit that separates both containers is removed and the gases allowed to mix, the reaction produces H_2O slowly because the collisions between the

hydrogen and oxygen molecules barely have the energy needed for the reaction to happen (it is a thermodynamically feasible process but not kinetically). If we introduce energy in the same system in the form of a spark the reaction accelerates. The energy needed for a reaction to happen is called activation energy E_A, by introducing the spark, we have injected energy into the system allowing for the rapid formation of H_2O.

The equation that relates changes in concentration with time is called the *rate law* or the *rate equation* of the reaction. For most cases, it is a function that associates the concentration of the reactants involved in the reaction and the respective changes of concentration over time for each reactant.

$$-\frac{d[A]}{dt} = -\frac{d[B]}{dt} = k\ f([A],[B]). \tag{1.1}$$

For reactions where reactants transform directly into the products, the form of the function f is simply the product of the concentrations of [A] and [B].

$$A + B \rightarrow C$$

$$-\frac{d[A]}{dt} = -\frac{d[B]}{dt} = k[A]^x[B]^y \tag{1.2}$$

Where k is the rate constant and contains the dependence of the kinetics with temperature, the sum of x and y allow us to obtain the total order of the reaction, that is, the relation between the speed of the reaction and the concentration of the reactants. Where x and y are known as the orders of the reaction for the corresponding concentration of the reactants [A] and [B]. A zero order kinetic means that changes in the concentration do not change the

speed of the reaction, A first order kinetic has a linear relation –doubling the concentration makes the reaction twice as fast–, and a second order happens four times faster by doubling the concentration and so on [34]. In general, the values of the rate constant and the order of the reaction (k, x, y) must be determined experimentally.

Reactions can also occur in a succession of steps, where the products of one step, becomes the reactants for a following one until the final products are produced. These reactions are called multi-steps kinetics, and studying a total multi-steps kinetics tells us about the slowest step that occurs, called the *rate-determining* or *rate-limiting* step [35] –the step with the highest activation energy E_A –, meaning that the formation of these products, limits the overall speed of the reaction, therefore a reaction can't happen faster than its slowest step.

One process that we can study with a kinetic approach is the nucleation and growth of crystals in solutions [36] [37]. Nucleation is an intermediate step process that allows the formation of a new thermodynamic phase, in this case a crystal. It starts when solute in a supersaturated solution forms small conglomerates, called seeds or nuclei of a new thermodynamic phase in the initial one by random fluctuations of the solute density, driven by an excess of Gibbs free energy in the solution that minimizes as the new phase starts to form. The crystal proceeds to grow from the aggregation of the solute in the solution to the nucleation sites in what is called the growth process [26]. The process of HZ/BH formation follows a nucleation and growth mechanism in the interior of the DV for the organic one and aqueous or aqueous-lipid solutions for the synthesized one. Living organisms exploit their ability to modulate the medium and the temperature where the crystallization occurs. In the case of *Plasmodium falciparum*, it has been suggested that the parasite uses the interior of the DV as a template for the crystal to grow faster by means of lipids present in the interior, accelerating (catalyzing)

the reaction, the formation of the crystal[38,39].

One way to represent the nucleation and growth mechanism is called classical nucleation theory (CNT)[40]. The most important assumption of this model is that the nucleation seeds are spherical and have the same structure as the macroscopic crystal[41]. There are other descriptions of the nucleation and growth, where more than one nucleation event is needed to form the precursors of the final crystalline phase (multistep nucleation models) but, those are not considered here given that there is experimental evidence that BH forms by a simpler CNT process[24]. Under this formalism, it is possible to find the limiting size at which a seed is stable and grows, called critical radius.

A way to think about the critical radius is that it characterizes the competition of the energy stored in the volume and the surface of a seed. The volume energy G_V tries to keep the structure together, and the energy of the surface γ , also called interfacial energy, tries to break it apart[26]. This occurs because the elements in the boundary are loosely bonded to the structure than the ones in the inner volume[26]. Following the previous discussion and taking the assumptions of CNT –modeling the seeds as spheres– lead us to:

$$\Delta G = -\frac{4}{3}\pi r^3 \Delta G_V + 4\pi r^2 \gamma,$$

where ΔG is the free-energy difference between the two processes.

The critical radius can be deduced as the minimum r at which the interfacial energy and the volume energy are equal:

$$r^* = \frac{2\gamma}{\Delta G_V}.$$

A model based on CNT, that represents the kinetics of the nucleation and growth, is the Avrami kinetic curve[42]. Relating the amount of material transformed from the initial phase to the new one as a function of time[43].

$$f(t) = A_0(1 - \exp(-kt^n)) \tag{1.3}$$

Where A_0 is the total amount of transformed material (in this case crystallized), n is proportional to the dimensions where the growth process occurs (for growth in one dimension nd=1, for 2D nd = 2, etc.) and if the nucleation occurs at different times (sporadic nN=1) or at the same time (instantaneous nN=0), with n =nd + nN, and k is a function associated to the nucleation and growth rates and seed geometry.

Authors have used the Avrami equation to study the kinetics of BH formation with and without antimalarials present[44,45]. In particular, Pasternack et al. *On the kinetics of formation of hemozoin, the malaria pigment*[1]. Proposed a model based on the Avrami equation and a simple exponential function to describe the kinetic curves of BH formation in an aqueous and aqueous-organic solutions:

$$Y = y_0 - y_1 \exp(-k\,t^n) - y_2 \exp(-k_s\,t), \tag{1.4}$$

where Y is the total conversion of hemin (heme with a coordinated bond between a chlorine atom and the central iron). y_1 and y_2 are the contributions made by the Avrami (fast process) and the simple exponential (slower process) with their respective rate constants k and k_s. This combination allowed them to represent the biphasic nature of the kinetic curves as a stretched exponential (see Equation 1.3) process that occurred very fast and a slower process

represented by the simple exponential curve, which is not fleshed out by the authors.

Other authors[46 19] have used the Avrami equation to represent the kinetic curves of BH formation when the antimalarial drug chloroquine is present. It is believed that chloroquine (CQ) works by adsorbing to the surface of the HZ crystal[25], slowing down the deposition of ferri-heme, be it on the entire surface or in the fastest growing faces of the crystal[47].

In the aforementioned models of crystal formation, there was an implicit assumption that the basic unit of crystallization is already present, and therefore it is a matter of seed formation and aggregation for the crystal to form in the solution. But, there is also the case that BH tends to self-associate in solutions, as it was pointed out by Klonis et Al.[20], where heme tends to interact via the porphyrin rings, forming π - π stacked dimers. Meaning that there must be an intermediate step in the BH formation process in solution where the μ-propionated dimers are formed and ready to form nucleation seeds and grow, producing the crystal[48]. The process of μ-propionated dimer formation could be considered as a rate-limiting step of the kinetics of BH formation. While Stiebler et Al.[45], proposed that the limiting factor in this step is heme solubility in the acidic medium, where the water molecules limit the formation of hydrogen bonds between the propionated groups of neighboring heme molecules and form the μ-propionated dimers. We propose that the formation of μ-propionated dimers from the π - π self-associated dimers is the rate-limiting step, that we modeled by a second order kinetic, where two π - π dimers must interact to form the μ-propionated one.

$$\frac{dY}{dt} = k_1 (\alpha - Y)^2 \tag{1.5}$$

where k_1 is the rate constant of the reaction, alpha is the total convention of π - π to μ-propionated dimers and Y is the number of μ-propionated dimers.

The solution to this differential equation is:

$$Y = \alpha - \frac{\alpha}{\alpha\, k_1\, t + 1} \tag{1.6}$$

As μ-propionated dimers are formed, the process of nucleation and growth takes over and can be modeled by an Avrami equation. Nonetheless, other options are available. In our case, we used a logistic curve to represent the process of deposition of μ-propionated dimers into the surface of a crystal.

$$\frac{dY}{dt} = k_2\, Y(\beta - Y) \tag{1.7}$$

Where k_2 is the rate constant, β is the total amount of crystallized material and Y is the amount of crystallized material.

The solution to this differential equation is:

$$Y = \frac{\beta}{1 + \exp(-\beta k_2\, t + D)} \tag{1.8}$$

The complete model of crystallization proposed in this thesis is presented here and derived in detail in Appendix C:

$$Y = \alpha - \frac{\alpha}{\alpha\, k_1\, t + 1} + \frac{\beta}{1 + \exp(-\beta k_2\, t + D)} \tag{1.9}$$

1.3 Computational Modeling

For the fitting of the two models, we used a trusted region reflective algorithm (TRF) implemented in the python library scipy, specifically the scipy.optimize.curve_fit implementation of the TRF method. The reason to employ it was that it is a robust method that allowed us to specify boundary conditions for the parameters in both models[49].

We used the Coefficient of determination R^2, Equation 1.10, as a measure of how good the models represented the data, the root-mean-square error RMSE and mean-absolute-percentage-error MAPE, equations 1.11 and 1.12, as dispersion measures of the models presented here (Pasternack 1.4 and SOM 1.9) and the experimental data in an aqueous and aqueous-octanol medium under the presence of the antimalarials artesunate and chloroquine at three concentration (0, 10 and 30 mg) each. $y_{exp,i}$ represents the ith experimental data point, $\overline{y}_{exp}$ the average of the experimental data points and y_i is the value generated by the fitted model.

$$R^2 = \frac{\sum_{i=1}^{N}(y_{exp,i} - \overline{y}_{exp})^2 - \sum_{i=1}^{N}(y_{exp,i} - y_i)^2}{\sum_{i=1}^{N}(y_{exp,i} - \overline{y}_{exp})^2} \tag{1.10}$$

$$RMSE = \sqrt{\frac{1}{N}\sum_{i=1}^{N}(y_{exp,i} - y_i)^2} \tag{1.11}$$

$$MAPE = \left(\frac{1}{N}\sum_{i=1}^{N}\frac{|y_{exp,i} - y_i|}{y_{exp,i}}\right) \times 100 \tag{1.12}$$

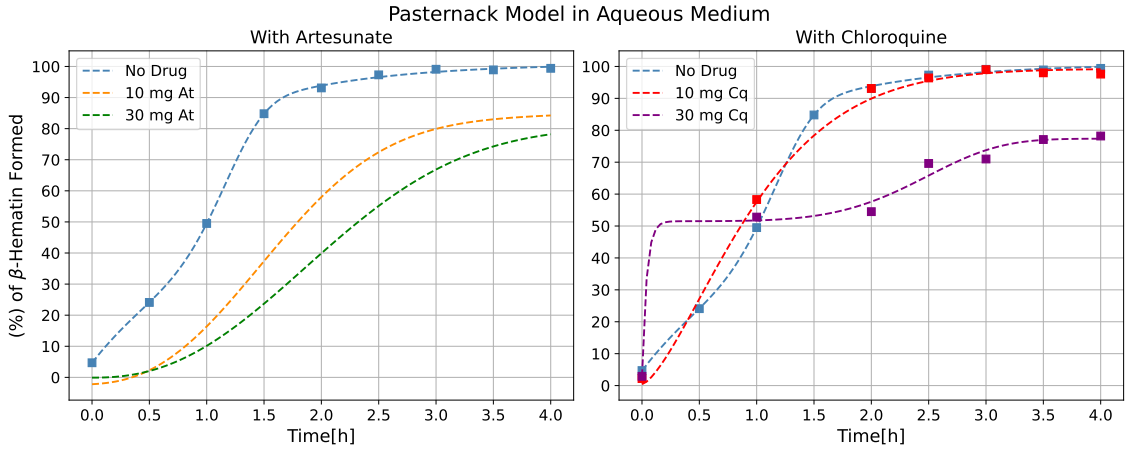

Figure 1.1: Experimental data (squares) available in Herrera et at[2]., with its corresponding fitted curves (dashed lines of the same color as the experimental points) of the crystallization process in an aqueous solution using the Pasternack model of crystallization, see Equation 1.4, (artesunate experimental points aren't shown, pending for publication). The introduction of the antimalarial reduces the overall total of crystallized material, except in the case of 10 mg of chloroquine, where the effect produced by the antimalarial is minimal compared with the non-antimalarial curve. But for the case of 30 mg of chloroquine, there is an entire hour where the material is not crystallized.

1.4 Results

We start our analysis with the aqueous medium in the presence and absence of antimalarials, see Figure 1.1. The solutions were studied for 4 hours. In which, the one without antimalarials crystallized 99.4% of the solute, compared to the 10 mg artesunate case, where the solution crystallized 85.8% of the solute, while the chloroquine solution, at the mentioned concentration, had a negligible effect on the crystallization process (97.6%). For the 30 mg concentration of the antimalarials, the total crystallized material, for artesunate and chloroquine solutions, are 77 and 78% respectively. Showing that the initial CQ concentration wasn't enough to produce a significant effect on the total crystal yield. The CQ concentration in-

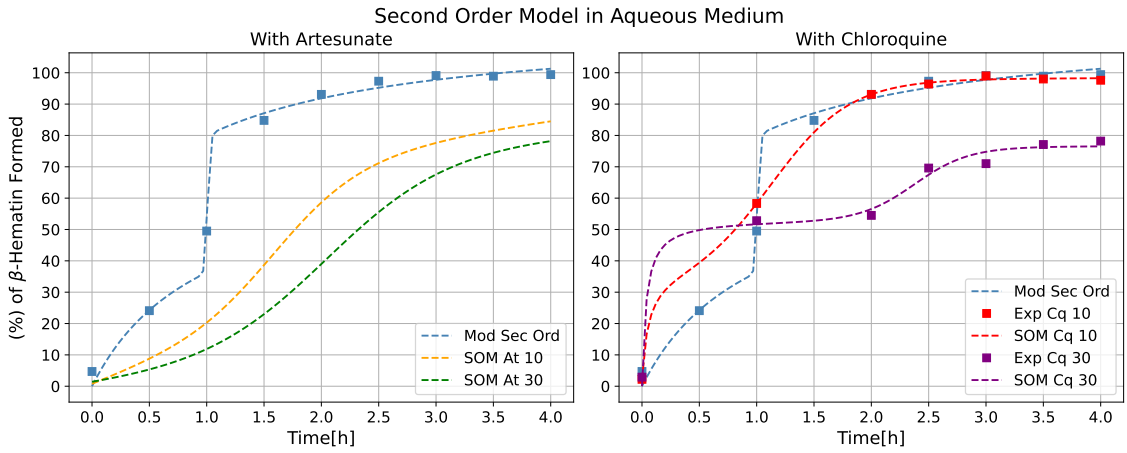

Figure 1.2: Experimental data (squares) available in Herrera et at[2]., with its corresponding fitted curves (dashed lines of the same color as the experimental points) of the crystallization process in an aqueous solution using the second order model (SOM) of crystallization, see Equation 1.9 (artesunate experimental points aren't shown, pending for publication). The introduction of the antimalarial artesunate slows down the crystallization process at first and gradually increases to its maximum value at 4 hours. The introduction of chloroquine is most noticeable in the 30 mg case, where the process stops for 1 hour.

crement, led to a total crystallization of 78% (comparable to the 30 mg artesunate case), but also halted it for 1 hour –between the 1-hour and 2-hour mark–. Hinting that chloroquine possibly acts by capping the surface of the crystal or binds to the fastest growing faces of it[47], as more capping material means less available sites in the nucleation seeds for the solute to adhere[38 22]. Here we suggest that this results could be improved with more experimental points in the region of 0 to 1 hour, improving the fit in this region.

Increasing the concentration of artesunate did not produce a halting in crystallization or any significant change to the kinetic curve, comparing the 10 and 30 mg artesunate curves reveals that the first concentration reduced the total crystallized material by 14% while the 30 mg one only reduced it by another 8%, suggesting a plateau in the efficacy of the antimalarial

with an increase in concentration. Both curves exhibit a strong effect in the beginning of the kinetics than at the end of it. This checks out with the observation that artesunate has a short-lived action time of 1 hour[50], where it sequesters free-heme and makes complexes with it[18 47].

The fitted models (Pasternack and SOM) presented a R^2 of 0.99 for the (no drug, 10 and 30 mg) concentrations with and without the antimalarials present, except the 10 mg artesunate Pasternack and SOM case with 0.98 and 0.97 % respectively. This means that both of the models represented fairy well the data in all the concentrations and the antimalarials. The chloroquine data had smaller RMSE and MAPE values than the artesunate case for both models and in the case of Pasternack, we argue that the model was originally used to represent the kinetics in the presence of chloroquine, not artesunate and therefore a small secondary mode of action of this antimalarial could be poorly represented by it, favoring the representation of the chloroquine data, and in the case of 10 mg artesunate, the initial data starts below zero. We do not ascribe any meaning to this and suggest that this particular curve could be improved by more data in this region, helping us fit the model to the data better, this can also be seen in the higher errors present in the parameters of this fit. For the R^2 and the dispersion measures and the mentioned data, see Table 1.1.

Both models represent successfully the data and have comparable errors, making both modes valid candidates to represent the kinetic data. If we compare the standard deviations of the fitted parameters for both curves, see Tables 1.2 and 1.3. It is clear that the Pasternack model has smaller values, but our model has 5 five parameters compared to the 6 used by Pasternack. The extra parameter allows a smoother representation of the no drug curve compared to the SOM, which describes a slow start followed by an accelerated crystallization

Aqueous Medium

Model	Antimalarial	R^2	RMSE	MAPE
Pasternack	No Drug	0.9998	0.498	0.3884
	10 mg Art	0.9833	4.0396	13.4985
	30 mg Art	0.9952	1.9388	4.7648
	10 mg Cq	0.9998	0.5011	0.3393
	30 mg Cq	0.9919	2.1891	2.6118
Second Order	No Drug	0.9964	2.0901	1.1927
	10 mg Art	0.9775	4.6901	18.0878
	30 mg Art	0.9934	2.2714	7.2302
	10 mg Cq	0.9998	0.5318	0.3509
	30 mg Cq	0.9915	2.2421	2.1668

Table 1.1: Statistical Parameters of the Models in Aqueous Solution

Pasternack Model Aqueous Medium

Antimalarial	y_0	y_1	y_2	n	k[1/h]	k_s[1/h]
No Drug	100.94±(0.90)	47.31±(3.14)	48.97±(3.96)	4.55±(0.41)	0.37±(0.04)	0.96±(0.08)
10 mg Art	92±(472.51)	80±(243)	14.20±(447)	2.40±(4.43)	0.23±(0.65)	0.16±(9.46)
30 mg Art	80.77±(6.11)	80.86±(52.30)	0.0±(52.92)	2.34±(1.22)	0.13±(0.15)	0.50±(0.0)
10 mg Cq	98.16±(4.20)	95.96±(20.25)	0.0±(24.30)	1.74±(0.34)	0.88±(0.07)	0.50±(0.0)
30 mg Cq	77.37±(4.74)	25.85±(8.32)	48.61±(8.54)	4.90± (4.20)	0.01±(0.04)	24.63±(0.0)

Table 1.2: Free Parameters of the Pasternack Model in Aqueous Solution

that slows down at the 1.5 hour mark. But other than that, the extra parameter doesn't help with the poor description of the first hour of the kinetics with chloroquine, where both the Pasternack and SOM show that the presence of the antimalarials accelerate the formation of the crystal, with the 30 mg chloroquine kinetics the most obvious case where the models fail to represent the data. This could be solved by having more experimental points in this region. Having said that, the artesunate case for both models represents smooth sigmoid curves that delay their crystallization strongly in the beginning and after one hour grow faster, in accordance with the short-lived action of artesunate.

We now continue our analysis for the aqueous-octanol solution by comparing the kinetic

Second Order Model Parameters

Antimalarial	α	k_1 [1/h]	β	k_2 [1/h]	D
No Drug	71.63±(12.21)	0.014±(0.006)	43.70±(6.68)	2.15±(0.32)	94.62±(0.0074)
10 mg Art	90±(272.50)	0.0016±(0.01)	51.70±(38.40)	0.05±(0.06)	4.20±(2.41)
30 mg Art	58.73±(883.73)	0.0011±(0.03)	67.85±(52.67)	0.03±(0.03)	3.84±(1.83)
10 mg Cq	34.43±(13.50)	0.5±(3.99)	64.32±(9.90)	0.05±(0.01)	3.34±(0.38)
30 mg Cq	53.30±(143.34)	0.8±(95.64)	22.98±(106.10)	0.24±(2.82)	12.81±(102.27)

Table 1.3: Free Parameters of the Second Order Model in Aqueous solution

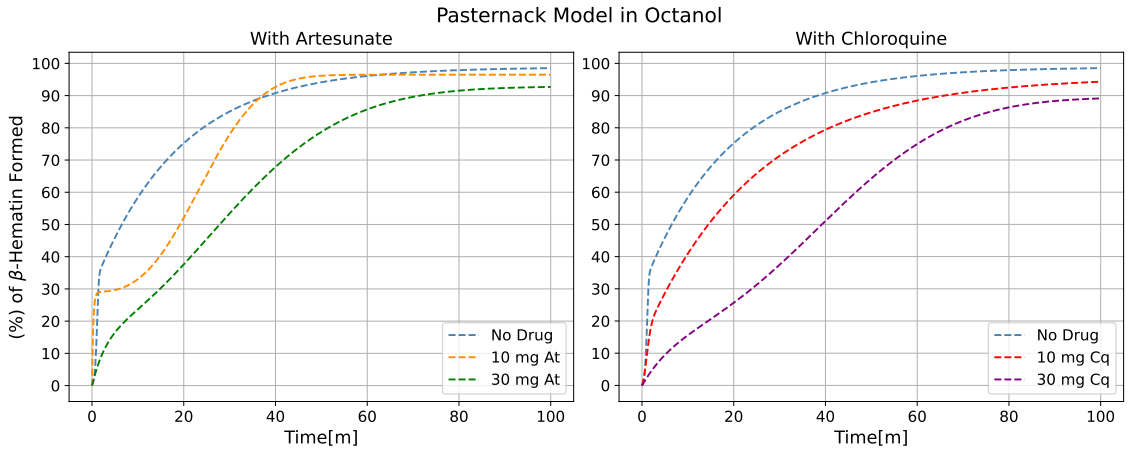

Figure 1.3: Pasternack model of crystallization in octanol. Experimental data not shown, pending for publication. Fitted curves (dashed lines) of the crystallization process under two concentrations (10 and 30 mg) of the antimalarials artesunate and chloroquine. The crystallization process takes 100 minutes.

curves in the aqueous and aqueous-octanol ones, see Figures 1.1, 1.3 and 1.2, 1.4. We notice that in the aqueous medium, the process took 4 hours for the no drug solution to reach its maximum value (99.4%). The same curve in the octanol medium took 100 minutes (2 hours and 20 minutes less than the aqueous one) to reach its maximum value of 98.92%. This behavior is congruent with the observation of Olafson et al., and others, that crystallization growth rate increases with solubility[24,45]. This also applies to the antimalarial cases, where the 10 mg artesunate and chloroquine aqueous solutions, reached respectively a crystalliza-

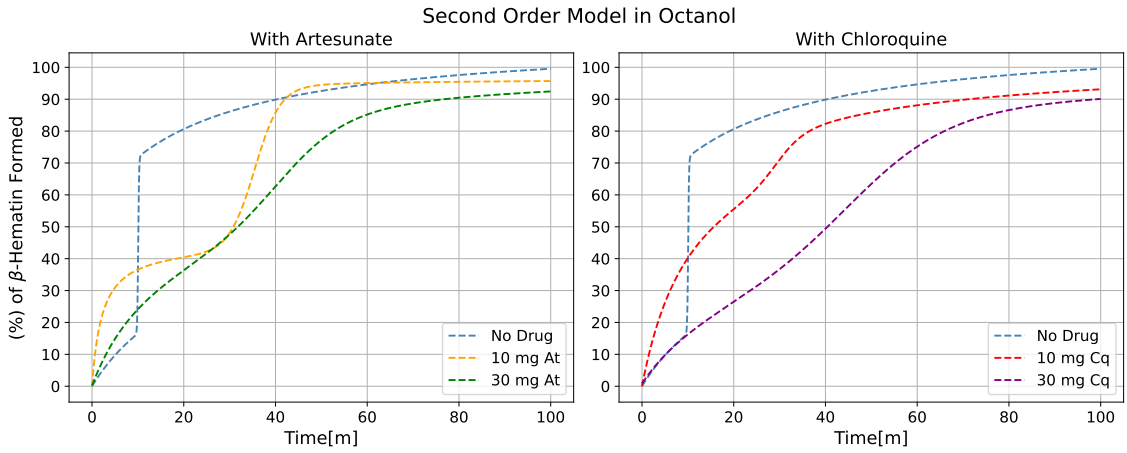

Figure 1.4: SOM of crystallization in octanol. Experimental data not shown, pending for publication. Fitted curves (dashed lines) of the crystallization process under two concentrations (10 and 30 mg) of the antimalarials artesunate and chloroquine. The crystallization process takes 100 minutes.

tion of 85 and 97% of the total solute, whereas the aqueous-octanol solutions reached 96.6 and 95.8% respectively. It is interesting to note two things: artesunate had a significant reduction of its performance (impeding the deposition of 11.6% less material in the aqueous solution) and chloroquine acted a bit better in octanol impeding the deposition of 1.2% less material and having a stronger effect that artesunate, something that didn't happen in the previous medium, we suggest that this occurs because chloroquine is more soluble in the octanol solution[24]. In the 30 mg cases, we also find that chloroquine acts marginally better than artesunate, crystallizing 89.5 and 92.8 % respectively. Comparing to the previous result with the aqueous media, where the crystallization reached 77 and 78% for the artesunate and chloroquine respectively.

It is clear that the medium plays a crucial role in the kinetics of crystallization, therefore mimicking as much as possible the conditions in the interior of the DV is important to un-

derstand the action of our current antimalarials inside the parasite and gauge effectively their action. Using octanol in the solution leads to the formation of interfaces between the aqueous part of the solution and the octanol, aiding in the formation of the crystal, as it was shown by Pasternack et al.[1] Who used another alcohols as co-solvents to mimic the interior of the DV, where lipids and the aqueous acidic solution interact. Authors suggest that the interface aids in the formation of μ-propionated dimers faster than the aqueous medium alone[48].

Comparing the R^2 of Pasternack and SOM we find that all of them reached 0.99, except the 10 mg artesunate case with 0.98, meaning that both models are comparable in describing the data, noting that ours uses one parameter less than Pasternack. Referring back to the dispersion measures, we see again that both models are comparable, and we can't choose one over the other, see Table 1.4. Checking the standard deviation of the fitted parameters for both models not only showed us smaller errors compared to the ones in the aqueous medium, but also that both models have comparable standard deviations with each other.

Returning to the crystallization models in octanol, we see that the no-drug curve in the Pasternack model is smoother than the one in SOM (as it was the case in the aqueous medium alone). In pasternack, the crystallization in the first 5 minutes of the kinetics occurs very fast and proceeds to gradually increase until the maximum is reached, this is dissimilar to the smooth growth observed in the aqueous case. For the SOM, the process starts slower for the first 10 minute, increasing gradually until the 10 minutes mark, where the process accelerates dramatically and then gradually reaches the maximum value. If we compare the no drug case for SOM in aqueous and aqueous-octanol, we see that the curves are remarkably similar, both having humps in the beginning of the kinetics, 0 to 10 minutes in the octanol and 0 to 1 hour in the aqueous one. We have to remember that forming μ-propionated dimers in the solu-

Oil Medium

Model	Antimalarial	R^2	RMSE	MAPE
Pasternack	No Drug	0.993	0.926	0.679
	10 mg Art	0.9806	4.666	4.1711
	30 mg Art	0.9967	1.8875	1.9533
	10 mg Cq	0.9954	1.9858	2.2906
	30 mg Cq	0.9984	1.3675	1.796
Second Order	No Drug	0.9984	1.154	0.936
	10 mg Art	0.9938	2.631	3.4136
	30 mg Art	0.9987	1.2123	1.8542
	10 mg Cq	0.9958	1.9105	1.9738
	30 mg Cq	0.9987	1.1075	1.8608

Table 1.4: Statistical Parameters of the Models in Octanol

Pasternack Model Parameters (Octanol)

Antimalarial	y_0	y_1	y_2	n	k[1/min]	k_s [1/min]
No Drug	99.92±(2.82)	29.92±(15.90)	69.99±(13.97)	3.98±(0.0)	0.5±(0.0)	0.05±(0.01)
10 mg Art	99.90±(3.25)	69.81±(9.90)	30.11±(11.24)	2.78±(1.06)	0.0001±(0.0002)	3.82±(0.0)
30 mg Art	100±(2.22)	79.60±(19.78)	20.40±(18.75)	1.89±(0.60)	0.001±(0.0024)	0.31±(1.21)
10 mg Cq	100±(2.37)	14.32±(7.81)	85.68±(6.19)	2.10±(0.0)	0.5±(0.0)	0.04± (0.006)
30 mg Cq	100±(2.01)	78.42±(15.07)	21.66±(13.95)	2.36±(0.53)	0.0001±(0.0002)	0.13± (0.15)

Table 1.5: Free Parameters of the Pasternack Model in Octanol

tion is needed for the material to crystallize, and therefore a slower kinetics in the beginning aligns with our intuition of the problem, given that, as the seeds form in the beginning of the kinetics, μ-propionate dimers need to form and bind to them in order of the crystal to grow.

We conclude this chapter by recapitulating that we were able to present here a new kinetic model of BH formation, able to represent the experimental data under different mediums and in the presence of different antimalarials, comparable to an existing model of BH crystallization, using fewer parameters and with an interpretation based on two stages: one based in the formation of the dimer units needed for BH to form and the other one in the nucleation, growth and eventual crystallization of the dimerized material.

Second Order Model Parameters (Octanol)

Antimalarial	α	k_1 [1/min]	β	k_2 [1/min]	D
No Drug	54.99±(15.87)	0.0008±(0.0005)	55.93±(20.48)	0.19±(0.07)	107.34±(0.0001)
10 mg Art	46.31±(10.53)	0.01±(0.02)	53.78±(8.43)	0.0069±(0.003)	12.71±(4.06)
30 mg Art	66.36±(22.34)	0.001±(0.0008)	42.48±(14.90)	0.0034±(0.0023)	5.45±(2.04)
10 mg Cq	90.44±(15.05)	0.001±(0.0004)	16.15±(10.28)	0.02±(0.05)	10±(19.60)
30 mg Cq	45.47±(26.83)	0.001±(0.0013)	53.19±(17.53)	0.0017±(0.0009)	4.12±(1.10)

Table 1.6: Free Parameters of the Second Order Model in Octanol

To see a World in a Grain of Sand And a Heaven in a Wild Flower Hold Infinity in the palm of your hand And Eternity in an hour ...

WILLIAM BLAKE

2

The IR Spectra of β-Hematin in the Presence of Chloroquine

2.1 Introduction

In this chapter, we use density functional theory (DFT) to simulate the infrared (IR) spectra of the BH dimer and compare it with experimental samples of the crystal in two scenarios, one

where the antimalarial chloroquine is absent and the other where it is present in the solution that produced the crystals. We do this by analyzing the vibrations (trajectories) generated in the simulation, comparing them with the experimental IRs and literature references to the characteristic peaks of the crystal. The comparisons were made in order to identify how the antimalarial affects the IR peaks and how our dimer model can help us identify missing peaks due to the presence of the antimalarial, not forgetting that this simplification doesn't allow us to characterize collective vibrations of the crystal and overestimates the peaks associated to vibrations between the dimers. The experimental data used here was provided to us in collaboration with the *Solid State, Residue Analysis and Malaria Research Groups, from the Faculty of Exact and Natural Sciences of the University of Antioquia*.

2.2 A Brief Introduction to DFT Methods and Its Application to IR

Solving the many-electron Schrödinger equation is a task computationally expensive that increases with the number of particles considered. In principle, all the information that we may need is present in the wave function of the system, therefore, the standard way to calculate the properties of a system of interest is to determine the potential $\sum_{i<j} U(\mathbf{r}_i, \mathbf{r}_j)$ associated with the interactions present in our system, solve the Schrödinger equation and obtain the wave function $\Psi(\mathbf{r}_1, \mathbf{r}_2, \ldots, \mathbf{r}_N)$, which we use to calculate the expectation value of a physical property that we want to understand, Equation 2.1.

$$\left[\left(\sum_{i}^{N} -\frac{\hbar^2\nabla_i^2}{2m} + v(\mathbf{r_i})\right) + \sum_{i<j} U(\mathbf{r}_i, \mathbf{r}_j)\right]\Psi(\mathbf{r}_1, \mathbf{r}_2, \ldots, \mathbf{r}_N) = E\,\Psi(\mathbf{r}_1, \mathbf{r}_2, \ldots, \mathbf{r}_N) \quad (2.1)$$

N is the number of electrons, m is the mass of the electron, $\hbar$ is the reduced Planck's constant and $U(\mathbf{r}_i, \mathbf{r}_j)$ is the electron-electron interaction term, in this case, the coulomb interaction:

$$\sum_{i<j} U(\mathbf{r}_i, \mathbf{r}_j) = \sum_{i<j} \frac{q^2}{|\mathbf{r}_i - \mathbf{r}_j|},$$

the potential of the system is:

$$\widehat{V} = \sum_i v(\mathbf{r_i}) = \sum_{ik} \frac{Q_k\, q}{|\mathbf{r_i} - \mathbf{R_k}|}.$$

Where Q_k and R_k are the nuclear charge and position of the k atom, respectively. Here we have evoked the Born-Oppenheimer approximation. Given that we are only working with the electron's degrees of freedom and treated the nuclear part as a parameter. The important consideration here is that the movement of the nuclei compared to the electrons is slow, and therefore we can decouple the electronic and nuclear motions and in effect consider the nucleus as effectively static compared to the electrons[51].

An evocative example of the scalability of the many electrons wave function is presented in the article *A bird's-eye view of density-functional theory*[52], in which an N electron wave function $\Psi(\mathbf{r}, \mathbf{r}_2, \ldots, \mathbf{r}_N)$ is represented in a 20 point mesh requires 20^{3N} values to describe the system (without considering the spin degrees of freedom). Increasing the number of points in the mesh and/or the number of particles leads to considerable constrains on the computational resources needed to calculate the properties of the system. Luckily for us, the most important theorem of the DFT formalism can help us with that, by considering the density of the system, $n(\mathbf{r})$, see Equation 2.2, as a key variable that we can exploit to calculate the properties of our system.

$$n(\mathbf{r}) = N \int d^3r_2 \int d^3r_3 \cdots \int d^3r_N \, \Psi(\mathbf{r}, \mathbf{r}_2, \ldots, \mathbf{r}_N)\Psi(\mathbf{r}, \mathbf{r}_2, \ldots, \mathbf{r}_N) \qquad (2.2)$$

The Hohenberg-Kohn Theorem:

The external potential $v(\mathbf{r})$ of the system is completely determined (except by an additive constant) by the electron density of a non-degenerate ground-state of an N electron system $n(\mathbf{r})$. It follows that the ground-state function Ψ_0 is also completely determined, and therefore all the properties of the system of interest.

The proof is simple. Let us consider two potentials $v(\mathbf{r})$ and $v'(\mathbf{r})$, both of which produce the same density $n(\mathbf{r})$, meaning that we have two Hamiltonian $\widehat{H}$ and $\widehat{H}'$, with the same ground-state density $n(\mathbf{r})$ and with different wave functions Ψ and Ψ':

$$E_0 < \left\langle \Psi' \middle| \widehat{H} \middle| \Psi' \right\rangle = \left\langle \Psi' \middle| \widehat{H}' \middle| \Psi' \right\rangle + \left\langle \Psi' \middle| \widehat{H} - \widehat{H}' \middle| \Psi' \right\rangle = E_0' + \int d\mathbf{r} \, n(\mathbf{r}) \Big[v(\mathbf{r}) - v'(\mathbf{r}) \Big]. \quad (2.3)$$

We can do the same as in equation 2.3 with E_0' and Ψ:

$$E_0' < \langle \Psi | \widehat{H}' | \Psi \rangle = \langle \Psi | \widehat{H} | \Psi \rangle + \langle \Psi | \widehat{H}' - \widehat{H} | \Psi \rangle = E_0 - \int d\mathbf{r} \, n(\mathbf{r}) \Big[v(\mathbf{r}) - v'(\mathbf{r}) \Big], \quad (2.4)$$

adding equation 2.3 and 2.4 follows:

$$E_0' + E_0 < E_0' + E_0 \qquad (2.5)$$

This leads to a contradiction, there can't be two different potentials that give the same density, meaning that the density contains the complete information on the system under observation, and therefore all observables are functional of the electron density of the ground

state.The density is a function of one variable and the wave function is a function of N vectorial variables, meaning that if we return to the 20 points mesh, we only need 20^3 values compared to the 20^{3N} for the wave function [52].

The Kohn-Sham Method:

Now that we know an exact computationally less expensive way to inquire about many-electron systems, we are going to introduce a scheme to make calculations. It is the Kohn-Sham method. The basis of it consists in considering an auxiliary system formed by N *non-interacting* particles of mass m.

The Schrödinger equation for each non-interacting particle is:

$$\widehat{h}_s\varphi_i = \left[-\frac{\hbar^2}{2m}\nabla^2 + v_s(\mathbf{r}) \right]\varphi_i = \varepsilon_i\varphi_i, \tag{2.6}$$

see Equation 2.1. $\varphi_i(\mathbf{r})$ is the single-particle orbital (of the non-interacting system), with the potential $v_s(\mathbf{r})$. The kinetic energy functional of the non-interacting system has an explicit dependence on the orbitals and is an implicit functional of the electron density.

$$T_s = -\frac{\hbar^2}{2m}\sum_i^N \int \varphi_i^*(\mathbf{r})\nabla_i^2\varphi_i(\mathbf{r})$$

The kinetic energy of the interacting system can be considered as the contribution of the non-interacting system $T_s[n]$ and a term associated to the correlation between electrons due to electrostatic repulsion $T_c[n]$. Where $T[n]$ is a universal functional, that is, independent of the potential (second Hohenberg-Kohn theorem), that can be solved using the variational principle.

$$T[n] = T_s[n] + T_c[n]$$

We can rewrite the interacting energy functional in terms of the non-interacting auxiliary system:

$$E[n] = T[n] + U[n] + V[n] = T_s[\{\varphi_i[n]\}] + U_H[n] + E_{xc}[n] + V[n], \tag{2.7}$$

where $U_H[n]$ is the Hartree energy:

$$U_H[n] = \frac{q^2}{2} \int d^3r \int d^3r' \frac{n(\mathbf{r})\, n(\mathbf{r}')}{|\mathbf{r} - \mathbf{r}'|},$$

$V[n]$ is the external potential of the system, and $E_{xc}[n]$ is the exchange-correlation energy contribution. It is associated to the difference of the interactive and the non-interactive kinetic energy $T[n] - T_s[n]$ and $U[n] - U_s[n]$. By applying the variational principle to the Equation 2.7, we obtain the Kohn-Sham equations, see Equation 2.6. Where the density of the system is:

$$n(\mathbf{r}) = \sum_i^N f_i \, |\varphi_i(\mathbf{r})|^2, \tag{2.8}$$

with f_i being the occupation of the i'th orbital.

2.3 Computational Modeling

As mentioned earlier, DFT is widely used to study many-electron systems[53]. In our particular case, it is used to simulate the IR spectra of atoms and molecules from first principles[30].

$$I_i^{IR} = \frac{N\pi}{3c}\left|\frac{d\boldsymbol{\mu}}{dQ_i}\right|^2,$$

where I_i^{IR} is the infrared intensity of the ith mode, $\boldsymbol{\mu}$ is the electric dipole moment of the atom/molecule under consideration, Q_i is the ith normal mode coordinate of the system, and c is the speed of light. We used the python package atomic simulation environment (ASE)[3] to generate the IR spectrum of the relaxed geometry of the BH dimer using the mentioned scheme. The code generates a displacement of 0.05 a.u in the positive and negative direction of each axis near the equilibrium geometry, calculating the forces given the displacement around the axes. From the diagonalization of the Hessian matrix the vibrational modes are obtained. The derivative of the dipole moment with respect of the coordinates is then obtained as finite differences of the energy as a response to an external electric field.[30]

The dimer structure was relaxed in a vacuum using the python package GPAW[4 54] to use the projector-augmented wave (PAW) method with a convergence criteria of $0.05\ \mathrm{eV/Ang^2}$, using the PBE exchange-correlation functional[55] and the correction vdW TS09[56] to represent van der Waals interactions.

2.4 Results

The experimental IR spectra consist of two samples, one without antimalarial and the other with 30 mg of chloroquine present, see Figure 2.2. The introduction of the antimalarial in the sample does not change the position of the peaks at the 1100 to 1800 $\mathrm{cm^{-1}}$ range. The characteristic peaks that appear in this region consist of the carboxyl group stretching at 1661 $\mathrm{cm^{-1}}$ being one of the most intense peaks present ($C = O$), followed by the 1206 $\mathrm{cm^{-1}}$ peak associated to the bonding of one carboxyl group to the central iron of one of the hemes

that constitute the dimer $Fe - O - C$. These peaks were compared to other IR spectra found in literature[32 31] and the simulated data generated by us (blue lines in the same data), see Figure 2.2. The dimer was used as a simplified model of the crystal and compare it to the experimental data, see Figure 2.1. The peaks obtained from the simulated dimers were used to corroborate the vibrations found in the literature and analize the possible behavior of the peaks that did changed.

In the case of the $Fe - O - C$ peak, the simulation reproduced it at 1165 and 1171 cm^{-1} (two values, corresponding to the two bonds in the dimer) with an underestimation of 45 cm^{-1} in relation to the experimental data provided to us. For the 1661 cm^{-1} ($C = O$) peak, the simulation finds it at 1643 and 1646 cm^{-1} an underestimation of 20 cm^{-1} . For the 1711 experimental peak, it reproduces it at 1764 and 1766 cm^{-1} , an overestimation of 50 cm^{-1} that we relate to the limitations of the dimer model, for the IR spectra of BH, given that this bond corresponds to the carboxyl groups of two neighboring dimers that make a hydrogen bond and grow the crystal. This was also concluded by Ali et at., who found this peak at 1825 cm^{-1} when they simulated the BH IR spectra[32] using the B3LYP functional.

In general, IR is used to identify the presence of the 1206, 1661 and 1711 cm^{-1} peaks and conclude that the sample is BH. We decided to go a bit further and analyze the spectra in the 2000 to 4000 range in tandem with our simulated spectra and tried to characterize the vibrations present in that region, because for the non-antimalarial case, three peaks are present in this region (2850, 2917 and 3299 cm^{-1}), that aren't present in the 30 mg chloroquine sample.

When we go to the simulated spectra and study the trajectories that appear in this range, we find small peaks associated to vibrations of the $C - H$ bonds in the vinyl and methyl

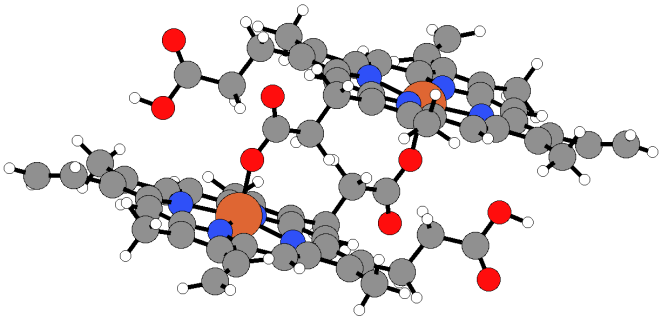

Figure 2.1: The β-hematin dimer used as a proxy to represent the entire crystal. With it, we can represent the most important bonds associated to the vibrations of the carboxyl groups in the dimer. The red spheres represent oxygen atoms, blue nitrogen, orange iron atoms, white are the hydrogens and gray the carbon atoms present in the dimer.

functional groups present in the porphyrin ring. We can see in Figure 2.2 that the simulated spectra overestimates these peaks[57] that correspond to $C - H$ vibrations. This could be due to limitations in the dimer model used to represent the BH crystal as in the case of the 1711 peak which was overestimated due to the lacking of the adjacent dimer that helps to produce an inter-dimer linkage bond, and it isn't present in the simulation because we only considered the dimer. For the 30 mg case, we decided to simulate the IR spectra of the chloroquine molecule, see Figure 2.4 in three different states of protonation (zero, once and twice protonaited), and compared to the experimental data of BH with the antimalarial present and found none of the peaks that the chloroquine simulated spectra produced, see Figure 2.3. in particular, the simulated peaks at 2831 and 3038 cm^{-1} correspond to intense $C-H$ vibrations, that were also found from other researchers who simulated the IR spectra of chloroquine around

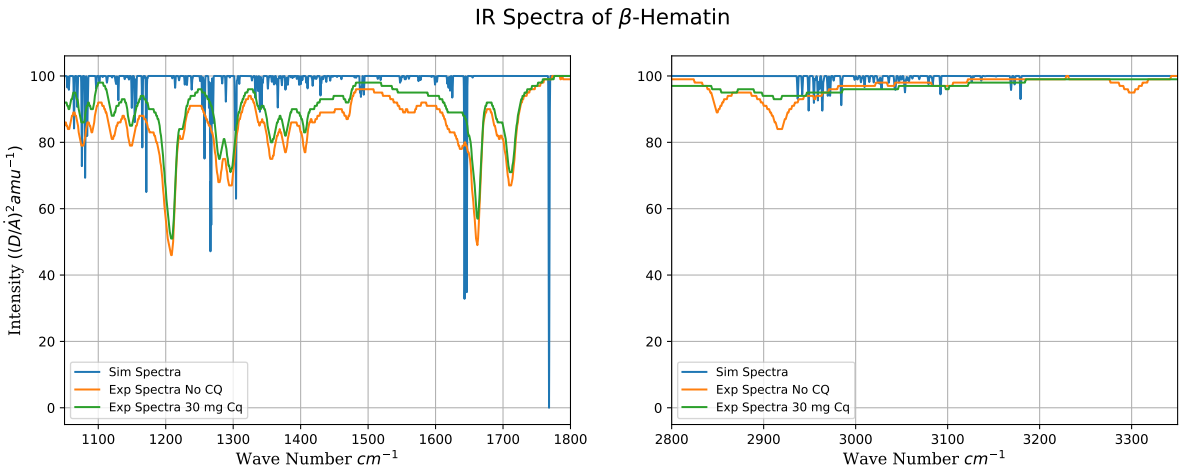

Figure 2.2: Experimental IR spectra of the BH crystal in the absence (orange) and presence (green) of 30 mg of chloroquine with the simulated IR spectra of the BH dimer (blue). The Experimental IR spectra (orange), shows the characteristic peaks of BH, corresponding to the vibrations of the carboxyl group and the central iron vibration associated to the formation of the dimer unit that span the crystal. The 30 mg chloroquine peak (green) shows the same position of the peaks if we compared to the no-drug case. The introduction of the antimalarial has no visible effect on the interior structure of the dimer by forming, breaking or displacing bonds. The only notable change is the disappearance of the 2850, 2917 and 3299 cm^{-1} from the 30 mg chloroquine sample.

2895 and 3259 cm^{-1} [58] and compared it to the experimental one at 2876 and 2993cm^{-1}.

This lends some support for the models of crystallization proposed by Crespo et al. and Klonis et al., who argue that due to the tendency of heme to self-associate in a solution [20], forming through $\pi-\pi$ interactions of the heme porphyrin rings, dimers. These dimers are the ones we argued in Chapter one, needed to transform into μ-propionated dimer, considered in literature as the agreed basic unit of BH formation [38], and we considered could be a rate-limiting step in the kinetics of BH formation. Klonis et al., goes further than us and considers that the BH crystal can be seen as a conglomerate of these $\pi - \pi$ dimers and the carboxyl linkage between dimer is not as strong in the pH of 5 of the DV in the parasite to form a

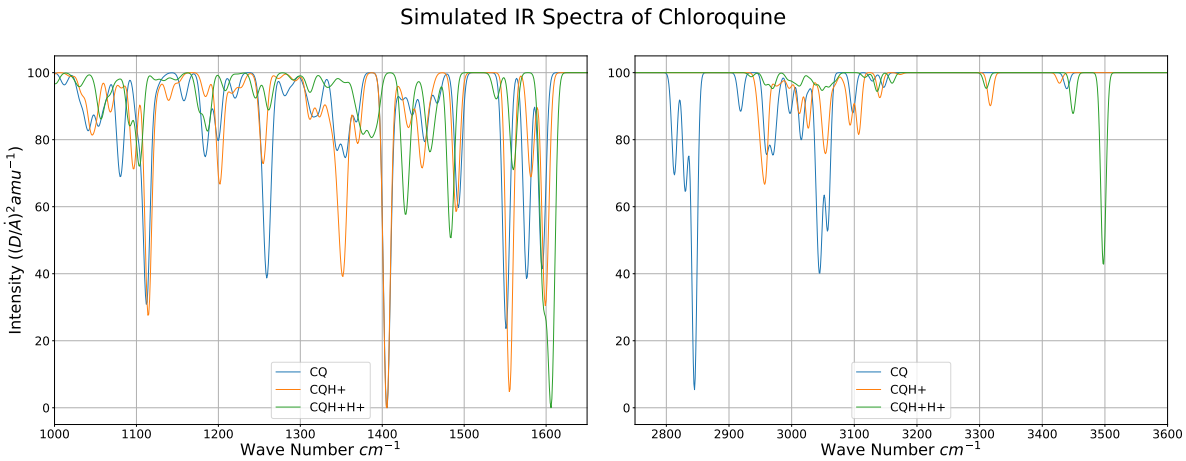

Figure 2.3: Simulated IR spectra of chloroquine, in three different states of protonation – non-protonated (blue), once protonated (orange), twice protonated (green)–.

stable dimer (the μ-propionated) and it is mostly a bond used to stabilize the structure in tandem with P-type interactions[20] that then proceeds to grow as 2D sheets that grow one on top of the other forming the crystal. Crespo et al., showed that the vinyl groups are crucial to the formation of the $\pi - \pi$ dimers[59], meaning that other type of interactions between the heme molecule and possibly the antimalarial involving these type of interactions would lead to slowing down the formation of the crystal. Checking the 2800 to 3300 cm^{-1} range, we see less interaction in these groups, possibly hinting at the loss interactions in the 30 mg case as interactions happening with the antimalarial in the sample. We of course can't be sure, with this analysis, that this is actually the case, meaning that more work is needed to settle this debate given the importance of understanding the mode of action of the antimalarial with the crystal structure.

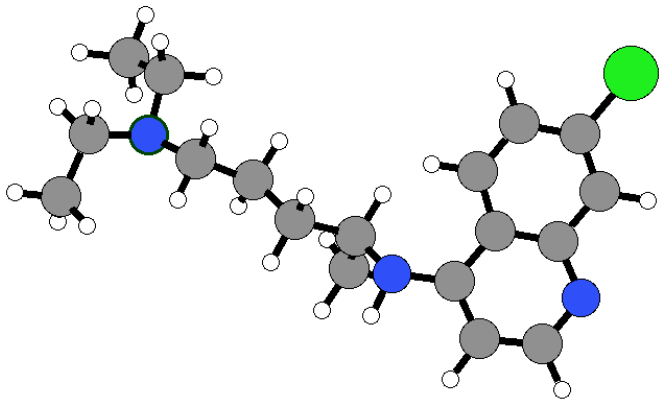

Figure 2.4: Structure of the Chloroquine molecule used to simulate the IR spectra used in this work. The carbon atoms are represented with gray spheres, the hidrogens with white ones, the nitrogen atoms with blue spheres and the chlorine atom with green.

Happy is the man who can recognize in the work of Today a connected portion of the work of life, and an embodiment of the work of Eternity. The foundations of his confidence are unchangeable, for he has been made a partaker of Infinity.

James Clerk Maxwell

3

Cellular Automatas: A Possible Model to Understand Crystallization

3.1 Introduction

In this section, we are going to delve into a possible alternative to studying the crystallization process of hemozoin/β-hematin, using a simple cellular automaton to represent the process

of nucleation and growth in a solution, applying the relation of the critical radius with the concentration of free-heme as a free parameter and relate it to changes in the crystallization behavior of the solute in the solution.

3.2 Generalities of the Cellular Automatas

Cellular automata are a parallel model of computation[60], meaning that we can understand how the output of a function is computed by the input given to it. In other words, we can use them to emulate the behavior of dynamical systems or by studying relevant properties of the automata and infer information of such systems. For our problem of BH crystallization, we can use a cellular automaton to emulate the behavior of solute particles in a solution (heme in a medium) and study the nucleation and growth process[33].

A cellular automaton is an object made of two components: First, a regular discrete network called the architecture, which is the space in which the system evolves in discrete time steps. Second, each node in the network, is called a cell. Each cell has a state associated to it (the possible states correspond to the specific problem in question). Each cell interacts with a finite number of local cells in a deterministic way (a set of rules), called a neighborhood. Given a cellular automaton in a particular time step. The transition between the current state of a cell and the next one –occurring in the next time-step– is defined by the current state of the cell and its local neighborhood. Under that definition, a cellular automaton can be considered as a machine that evolves with time[61].

The most famous cellular automaton is "The Game of Life", published in 1970 by John Conway[62]. Where 2 states –dead and alive– characterize the possible states of each individual cell. When a dead cell is adjacent to exactly 3 alive neighbors, in the next time-step the cell

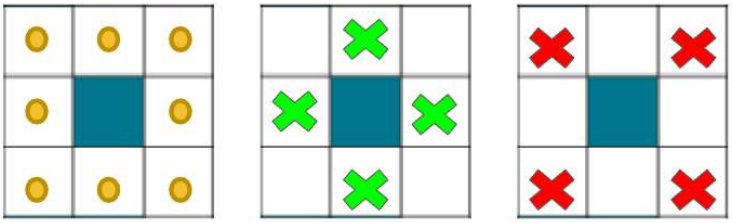

Figure 3.1: Different configurations of nearest neighbors that can be used to study the nucleation process. The blue square corresponds to the cell under consideration. For the first image, all the possible positions of the gold circle represent a site where a solute square is considered a neighbor. For the second and third neighborhood, only the positions of the green and red X are considered as neighbors.

will have the state alive. If an alive cell has 2 or 3 neighbors, then for the next iteration it continues to have the state of alive. Finally, if an alive cell has 4 or more neighbors with the state alive, then in the next iteration it will have a state of dead –as if overpopulation killed the cell–. If the number of alive neighbors is 1 or none, the cell in the next iteration will have a state of dead –as if isolation killed it–. From this simple set of rules for the assignation of a new state of the system, the game of life presents complex emergent behavior, such as stable configurations along the entire game (do not disappear as time progresses)[63].

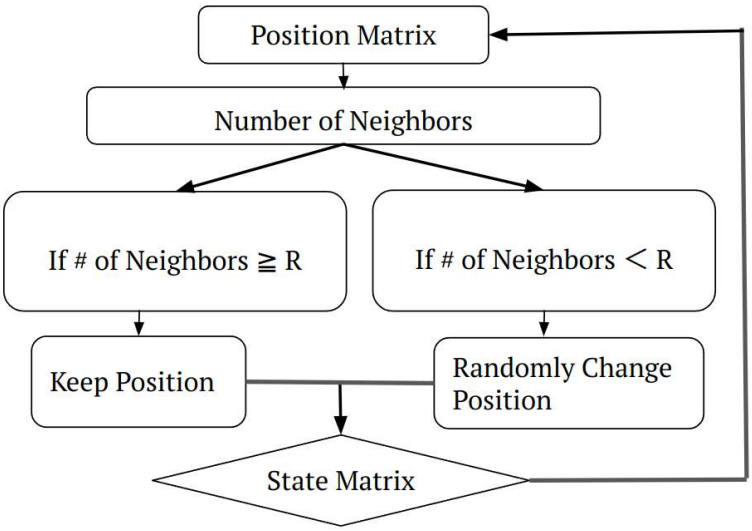

Figure 3.2: Neighbor rules followed by each cell of the cellular automaton. Given a solute cell, we count the number of solute neighbors. If the number of neighbors is equal to the critical radius R, then that cell keeps its position on the grid. If the number of solute neighbors is less than the critical radius, then the state of solute of this particular cell will be randomly assigned to one of the cells with the state solution. Keeping the number of solute states constant in the entire run of the simulation

3.3 Computational Modeling

We took as a starting point the "Game of Life" implementation done by the GitHub user Josephbaku-Likira, from the repository: https://github.com/Josephbakulikira/Conway-s-Game-of-life—Python. The game of life doesn't have a limit on the number of alive or dead cells that can be at a given time step, due to the possibility of dead/alive cells changing their state from dead/alive to alive/dead if the number of neighbors is big enough.

In BH formation solutions, the amount of solute is known, and it doesn't increase as the reaction takes place. Therefore, we modified the code to introduce a fixed number of states in the cells defined at the beginning of the code (we used a $120\times$ 90 grid). A portion of the

cells begin with the state solute, and the rest of them will be solution.

For the cellular automaton to work, we needed to define a neighborhood. Three candidates were considered as the neighborhood of our cells: The first one consists of all the cells one unit apart from the cell under evaluation (eight cells), The second consists of all the cells in the vertices of the cell (four cells) and finally, all the cells that were not in the vertices (four cells), see Figure 3.1. For the simulations presented in this work, we used the neighborhood that considers all the possible rectangles that are in contact with the studying cell (in this case 8). In the CNT formalism, the nucleation seeds have a spherical shape, and this was possible to obtain using the selected neighborhood.

The rules to update the states of the cells from one time step to the other are as follows: If the number of solute neighbors is greater or equal than the *critical radius*, see Chapter 1, Equation 1.2, then the cell keeps its state as solute. If the number of neighbors is less than the critical radius, then for the next iteration the state of the current cell will change from solute to solution and the unassigned solute state will be given randomly to one of all the current cells with the state solution (keeping the number of cells with the state solute constant in any time steps). Finally, if the state of a cell is solution, then it keeps that state unless it is randomly selected to replace a recently demoted solute state, see Figure 3.2.

From chapter 1, that when a crystallization seed is forming, there is a competition between the interfacial energy γ of the surface of the seed that tends to break the nucleation site apart with the bulk of the seed that is trying to keep it together. The size at which both contributions to the Gibbs free-energy (G) are equal, is called the *critical radius*, and it is a measure of stability for the seed formation process. Meaning that if a configuration has a size greater or equal than this radius, then the seed will continue to grow:

$$r^* = 2\frac{\gamma}{\Delta G}.$$

The Gibbs free-energy in a solution relates to variations of the chemical potential μ and the reactant (solute) concentration σ:

$$\Delta\mu = K_B\, T \ln(\sigma).$$

We can then describe the critical radius as:

$$r^* = 2\gamma/\Delta G = 2\gamma\Omega/K_B\, T \ln(\sigma) \tag{3.1}$$

Following Olafson et al.[24], we can represent the concentration σ as the hematin concentration c_H and hematin solubility c_e.

$$r^* = \frac{2\gamma\Omega}{K_B\, T \ln(c_H/c_e)} \tag{3.2}$$

Here, Ω is the volume of the hematin molecule, K_B is the Boltzmann constant and T is the temperature in kelvin. We used values found in the mentioned Olafson et al. reference for the parameters γ, c_e, Ω and T, leaving c_H as a free parameter for the simulation. In it, the value of c_H is used to assign the percentage of total cells that will be able to have the state solute in the simulation, leaving the rest with the state solution. As we mentioned early, this is an important departure from the original game of life, in which the number of alive/dead cells can vary over time.

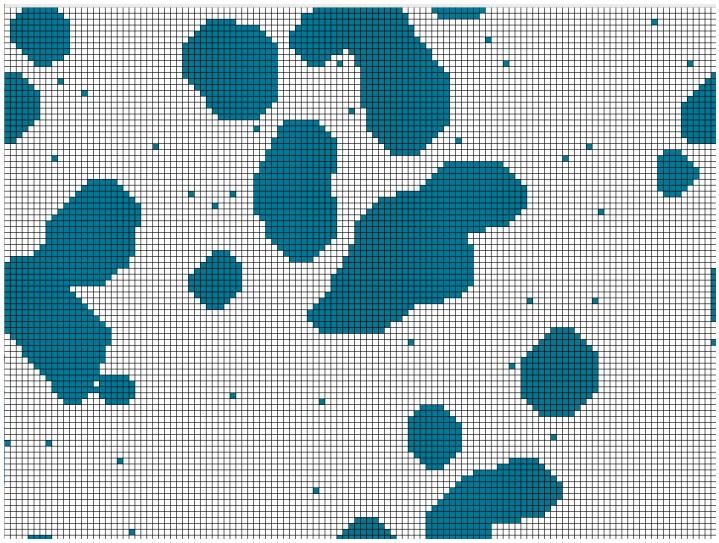

Figure 3.3: Cellular automaton simulation at a 16% concentration of heme in the solution. Here the nucleation seeds are big, and tend to be in proximity to one another. By imposing the rule of neighbors, which considers all the cells in contact with the cell under observation. We have imposed a symmetry on the system. See that some seeds are circular and the ones that deviate from it can be considered circular seeds that grew into one another, forming more elongated structures.

3.4 Results

By interpreting this cellular automaton as a 2D section of the solution, where the number of solute particles is constant as material enters and leaves the area of observation. Nucleation seeds form and dissolve until sufficiently large fluctuations produce and continue to grow, some of them as material adheres to its surface. Using this interpretation of the cellular automaton we proceeded to run a simulation where 16% of the total number of squares (120×90) correspond to solute (heme), available to form seeds, see Figure 3.3. By plotting the values in equation 3.2 with $c_H = 0.16$, we obtain a critical radius of 4. That is, we need four solute particles in the neighborhood of the observation cell to keep its state in the next iteration.

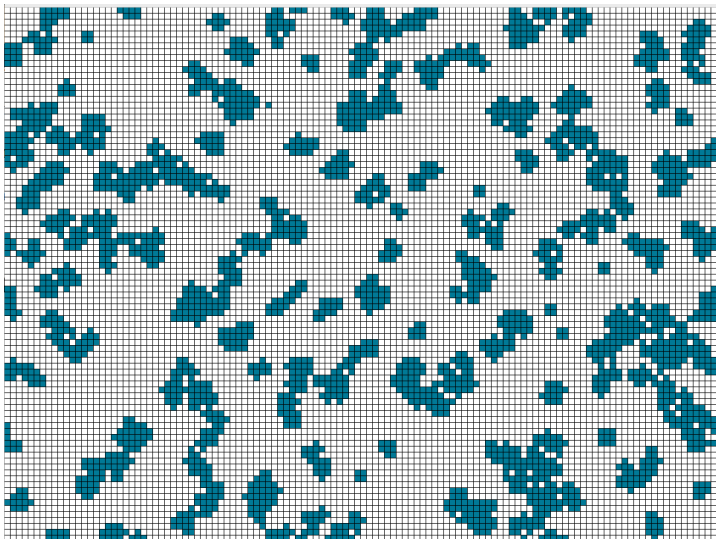

Figure 3.4: Cellular automaton simulation at a 20% concentration of heme in the solution. The nucleation seeds (lumps of blue rectangles) are small and dispersed around the entire simulation grid. This is in accordance with a small critical radius, meaning that the formation of the clumps happens quickly and uniformly in the entire simulation grid. This is similar to an instantaneous nucleation process[43].

Meaning that as the concentration becomes lower, the chances that by random fluctuations a stable seed is formed, becomes smaller. For our particular case, the seeds that appear here are almost spherical. This can be attributed to the use of a neighborhood that treats as equal all its possible nearest neighbors, see first neighborhood from Figure 3.1. This is congruent with the use of CNT, where the shape of the cluster is assumed to be spherical. If we look closely, we also find that the clumps present are formed as a composition of circular seed that were close to each other and grew into one another. As the surface (perimeter) of the clusters becomes bigger, it is easier to adhere loose molecules that haven't been able to adhere to a seed, therefore making it easy to grow and become a likely site for other loose molecules to adhere. This behavior leads to the formation of big clusters, that are close together, followed

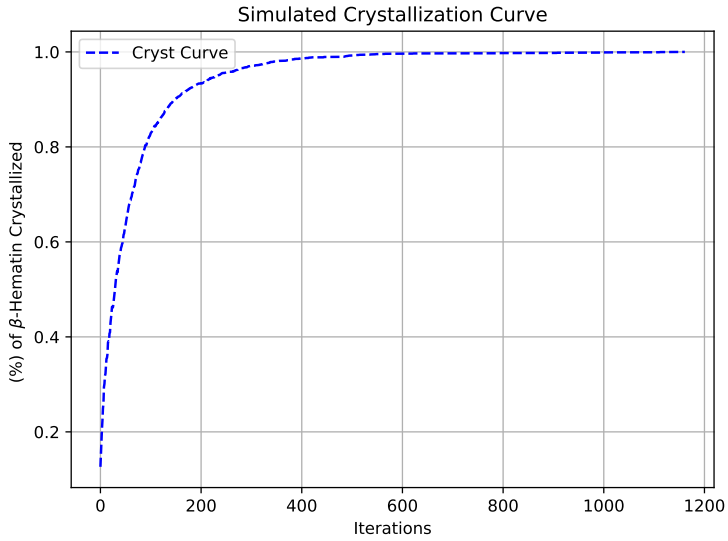

Figure 3.5: Curve generated by the cellular automaton simulation, with a heme concentration of 16%, meaning that 16% of the cells had the state solute. The x-axis of this graph shows the passage of time as iterations done by the automaton to reproduce the current state of the crystallized material. Here, we reached 100% at approximately 600 iterations.

by some smaller clusters in the periphery.

Increasing the percentage of heme in the solution from 16 to 20%, does not change the calculated critical radius from before (4), see Equation 3.2. But, the morphology of the seeds does change, see Figure 3.4. Now, we see smaller seeds that cover the entire grid. There are not favored places as the increase in solute means an increase in the likelihood that 4 solute molecules are near to form a site in any site of the simulation (the total number of squares in the simulation is the same (120×90) and the number of neighbors needed is the same). As the material spreads out more evenly around the grid, the formation of large conglomerates of seeds is not seen. We do not see unbound molecules in this scenario, in contrast to the 16% one. This means that the material crystallized faster as more surface area was covered by this

small but abundant configuration of seeds, making it a more suitable scenario than the last one. Here, it is also apparent that the morphology of the seeds is spherical, as we pointed out in the previous case, this could be ascribed to the choice of neighborhood. We can go further and propose that between the 16% and 20% case, we are experiencing different scenarios of nucleation in the solution.

The rapid formation of seeds in the entire solution is characteristic of instantaneous nucleation processes. This happens, when the formation of the seeds occurs in the entire solution at once[43]. While the case at 16% could be described better by a sporadic nucleation process, meaning that the formation of the seeds occurs at different times in different regions of the solution. Looking at the differences in the spreading of the material between the two cases, see Figures 3.3 and 3.4. We can see how the variation in the solute could influence these two types of nucleation behavior in the simulation.

Finally, as we sweep the entire grid each iteration to assigne the next state, we count the number of cells which are in the solute state that need to be reasingned randomly, meaning that we know in each iteration the number of non-interacting solute molecules N_{non} and by extension, the number of crystallized/interacting solute one $N_{int} = 1 - N_{non}$, allowing us to plot the number of iterations versus the crystallized percentage of one run of the automata –the crystallization curve of the system–, see Figure 3.5.

Comparing the previous result with an experimental curve of crystallization in 1-hexanol, taken from the Pasternack et al. paper *On the kinetics of formation of hemozoin, the malaria pigment*[1], see Figure 3.6, we find that the behavior of the curves is similar, as both of them experience a rapid growth, that tampers as the crystallized material becomes scarce and the amount of deposited material for unit of time becomes smaller. These similarities suggest

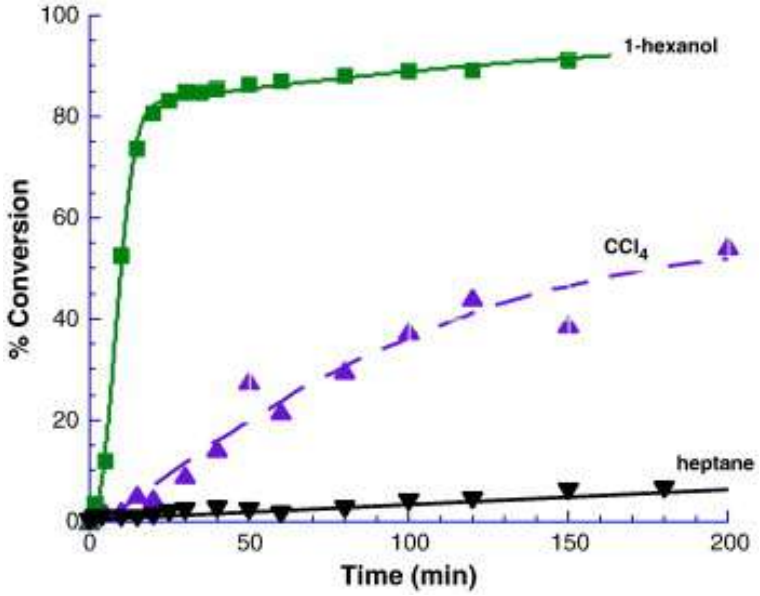

Figure 3.6: Graph taken from Pasternack et al. paper *On the kinetics of formation of hemozoin, the malaria pigment*[1]. Here we see the effect of co-solvents and its effect in the kinetic profile of hemin convention into hemozoin. This graph is reproduced here because the profile for the 1-hexanol resembles the crystallization curve generated by the cellular automaton.

that maybe if we can incorporate other elements present in the solution to the simulation, we can refine these results and be able to describe with more accuracy the formation of seeds, the crystallization time needed for the formation of the crystal and to analyze these variables when there are antimalarials present in the solution. This toy model for crystallization ultimately is another avenue to explore and analyze the factors involved in the formation of the BH crystal in a controlled and systematic manner, where the parallelization of the cellular automata can lead to bigger grids, avoiding pitfalls such as having a global depletion of the solute[64]. This implementation could lead to computationally available ways to attack problems that are similar to the crystallization problem that we explored in this section.

4

Conclusion

In this work, we presented a new model for β-hematin crystallization based on the classical nucleation theory (CNT) which represents the crystallization kinetic data as effectively as other models of crystallization seen in the literature such as the Pasternack model. We also, showed how the change in the medium reflected changes in the errors on the parameters of the fitted data. We attribute this behavior to the fact that crystal rate formation is proportional

to the solubility of heme and in the faster growing medium it is easier to see the effects of the antimalarial artesunate, which as a half-life of approximately 1 hour, this could be seen in the kinetics curves, where the effect of the artesunate was most notable in this region. For the chloroquine case, we see that when we are in the octanol medium, the antimalarial effect is seen on the time of the reaction, taking much longer to crystallize the material, but the effects of heme capture and the halting of the crystallization process were only observed in the aqueous case.

In the same line, we also tested a simulated IR spectra of the β-hematin dimer and compared it to a sample of crystallized β-hematin and found that the representative peaks at 1200, 1660 and 1710 cm^{-1} appeared, meaning that our simplification allowed us to represent the crucial elements in the experimental spectrum associated with the carboxyl group bonding to the central iron (1200 vibration), or the stretching of the $C = O$ bond of the carboxyl group bonded to the iron (1660) and the 1710 (Hydrogen bridge formed between free carboxyl groups in heme), which incidentally was overestimated because we did not include another dimer or carboxyl bond joint to it, which is consistent with other attempts to simulate this particular peak only using the dimer. Seeing that our model predicted fairly well the experimental peak at the 100-2000 cm^{-1} region of the IR. We used it to identify the possible vibrations that appeared in the spectrum at 2880 and 2930 cm^{-1} and that disappeared in a measurement of a β-hematin crystal grown with 30 mg of chloroquine present in the solution. The assignation of these peaks in our simulation corresponded to the methyl and vinyl groups in the porphyrin ring of the dimer. Given that, the vinyl groups are the most reactive. Research has indicated that it is fundamental for heme self-association, we propose that the absence of these peaks could mean that the chloroquine that bonds to the crystal

(capping mechanism) also interacts with these groups, in particular the vinyl group. This interaction of the antimalarial chloroquine and its role in the self-association process, lends some strength to our model of crystallization where the formation of the $\pi - \pi$ dimers is a possible rate-determining step that can be affected by the presence of the antimalarial that compete for the interaction with the vinyl group.

Finally, we used a toy model for crystallization based on cellular automata, in particular, Conway's game of life with modified rules to represent the process of nucleation and growth under the CNT approximation using the concentration of heme as the free parameter of the simulation. Here we compared the behavior of the curve of stationary heme units to the number of iterations and found that it is similar to some crystallization curves of 1-octanol, methanol, chloroform with lipids.The experimental data that we used were obtained from a lipid-based solution for β-hematin crystallization. The cellular automaton model was severely limited by the range of concentrations that we could explore because of computational limitations to expand the number of cells in the simulation and the number of neighbors that each individual cell could be assigned and computed. Nonetheless, this simple model was able to produce nucleation seeds of different sizes by modifying the critical radius as a function of heme concentration. Hinting at possible ways in which this avenue could be explored again using parallelization and better local neighborhoods to explore the crystallization process more broadly.

5

Perspectives

This work introduced a crystallization model under the assumptions of CNT, that considers the dimer formation process and takes it into account to model the kinetics of crystallization. This model could be used in other solutions in which the self-interaction of the solute is present, followed by a nucleation and growth stage. By taking into account the self-interaction of the solute and modifying the chemical environment of these molecules in the

kinetics, the model could aid identify the strength of such interaction. In the case of inhibitor agents being present in the solution, studying changes to the parameters could also help identify which of these processes (self-interaction or nucleation and growth) is affected the most.

For the IR-spectra study of the dimer under different concentrations of the antimalarial CQ, we propose that this methodology could be used for other chloroquine and artemisinin based antimalarials such as bromoquine and artesunate[38]. Analyzing the bonds as the concentration increases could be a useful guide to analyze dose dependent inhibition in these drugs and a possible guide to interaction sites between these molecules and the dimer. Following this thread, this work could be expanded by considering crystal sections bigger than the dimer. This would provide a wider picture of the behavior of the dimer, allowing us to represent the 1710 cm^{-1} peak better, and consider interactions due to collective vibrations of the selected slabs[65]. Their possible role in the interaction of the crystal with the antimalarial is still not clear, and we suggest that these expansions to the present work could shed light into these questions.

Finally, we used a cellular automaton to model the process of nucleation and growth of BH and found preliminary success representing the formation of the nucleation seeds. We propose that a GPU implementations of the cellular automaton would lead to a higher number of cells available to simulate, allowing us to explore a wider range of solute/solution concentrations and their effect in the formation of the nucleation seeds[64], helping us implement a random parameter proportional to interfacial energy of the BH molecule in solution[24] to accept or reject the union of any two pairs of cells in the boundary of the clusters present in the simulation and allow us to introduce other states to the cells in the simulation without increasing the computational demands, such as chloroquine or artesunate states, which

could represent the proposed behavior of these drugs and analyze their effect in the simulated kinetic by appropriate neighborhood rules of these and the solute states, helping us compare it to experimental data.

A

Products of this thesis

The academic products of this research are presented here. The first page of the papers and the poster are attached in the next pages.

- (Article) Julieth Herrera, **Cristian Parra**, Daniel Coronado Cardona, Valentina Perez, Julian Zapata, Adriana Pabón, Olga Lopez-Acevedo, Karen García, and César Barrero Meneses.Revising the formation of β-hematin crystals from hemin in aqueous-acetate

medium containing chloroquine: Modeling the kinetics of crystallization and characterizing their physicochemical properties. Crystal Growth & Design, 2023.

- (Article in Progress) *Julieth Herrera, ***Cristian Parra**, Olga Lopez-Acevedo, Karen García, and César Barrero Meneses, Julian Zapata.Applying two kinetic Models to β-Hematin Formation in the Presence of the Antimalarials Artesunate and chloroquine

- (3 Months Internship) **Cristian Parra**, Max Planck Institute for Biophysics, Theoretical Biophysics group, directed by Prof. Dr. Gerhard Hummer, under the supervision of Dr. Sergio Cruz-Leon

- (Poster) **Cristian Parra**, Olga Lopez-Acevedo. A Toy Model for the Crystallization Process of the Malaria Pigment Hemozoin. Event: Third University Symposium of Chemical research (3 SUQUI)

- (Speaker) **Cristian Parra**, Olga Lopez-Acevedo. A Toy Model for the Crystallization Process of the Malaria Pigment Hemozoin. Event: XXIX National Physics Congress

CRYSTAL GROWTH & DESIGN

pubs.acs.org/crystal

Article

Revising the Formation of β-Hematin Crystals from Hemin in Aqueous-Acetate Medium Containing Chloroquine: Modeling the Kinetics of Crystallization and Characterizing Their Physicochemical Properties

Julieth Herrera, Cristian Parra, Daniel Coronado Cardona, Valentina Perez, Julian Zapata, Adriana Pabón, Olga Lopez-Acevedo, Karen García, and César Barrero Meneses*

Cite This: https://doi.org/10.1021/acs.cgd.2c01429

Read Online

ACCESS | Metrics & More | Article Recommendations

ABSTRACT: We investigated the kinetics of conversion of hemin to β-hematin in aqueous-acetate medium in the absence and in the presence of two concentrations of chloroquine by using 11 reported kinetic equations. The two best kinetic equations are the combination of order 1 and Avrami and the combination of second order and logistic equations, based on the statistical parameter variance and overall errors. The best fitted equations are composed of two terms from which we model the formation of β-hematin as the result of two processes: the availability of reactive precursors and the formation of nucleation and growth sites. The crystals exhibit needle-like morphologies about 760-nm-long and 140-nm-wide. However, the increment of chloroquine favors the formation of crystal twinning with nonhomogenous distribution, crystals with lower sizes of similar heights and widths, and crystals symmetrically tapered at the ends of the needles. The lattice volumes, obtained from Rietveld analysis of powder X-ray diffraction patterns, were not regularly affected by chloroquine. The main IR absorption bands did not appreciably change in positions nor in intensities with varying chloroquine concentration. However, important changes were observed in the 2000−4000 cm^{-1} region. We used density functional theory calculations to understand these changes.

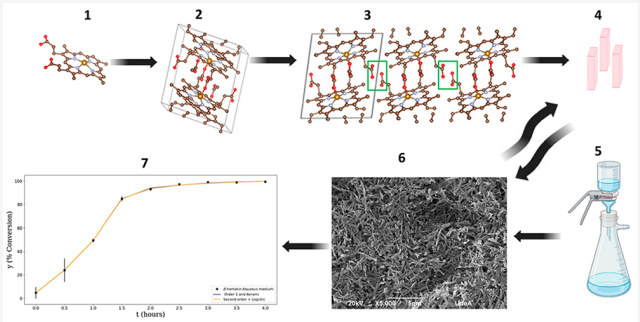

1. Hemin precursor. 2. β-hematin dimer. 3. Assembling of dimers. 4. β-hematin crystals. 5. Obtaining synthetic hemozoin (β-hematin). 6. SEM of synthetic hemozoin. 7. Best kinetic models.

INTRODUCTION

Plasmodium is a parasite that is transmitted to man by the bite of a mosquito of the genus *Anopheles* and causes malaria. This remains a significant public health problem. The World Malaria Report 2021 estimated that the global malaria burden was around 241 million reported cases and 496 000 deaths worldwide. To date, there are six species of *Plasmodium* that affect humans; however, *P. vivax* and *P. falciparum* are the most important. *P. vivax* is widely distributed and occurs mainly in the Americas, and *P. falciparum* is the species that causes the highest number of complications and deaths.[1]

During the life cycle of *Plasmodium* in the human host, it has an intraerythrocytic phase, which is related to the symptoms of the disease. In this cycle, *Plasmodium* degrades hemoglobin and after several processes forms the hemozoin crystal, or malaria pigment. It is widely accepted that the formation of the hemozoin in the digestive vacuole of the *Plasmodium* parasite is the primary mechanism of heme detoxification in the malaria parasites and the target of quinoline type of antimalarials.[2−4] Therefore, it is very important to have a deep understanding of the formation mechanisms and kinetics of nucleation and growth of the hemozoin crystals and their inhibition by the antimalarial medicines. These types of studies have been performed on both natural and synthetic samples, the methods being valuable and complementary.

The synthetic version of the hemozoin crystal is called β-hematin, and it can be synthesized under widely different conditions. One of the earliest reactive mediums used to synthesize β-hematin was acidic acetate solutions.[5−8] Egan and co-workers[5,6] reported short reaction times for the formation of about 30 min under the reaction conditions of 4.5 M acetate buffer, pH = 4.5, and a temperature of 60 °C. The reaction was also complete within 2 h at 37 °C and 8 days at 6 °C. In 1993,

Received: December 3, 2022
Revised: May 20, 2023

VERWALTUNG
UND ALLGEMEINE SERVICES

MAX-PLANCK-INSTITUT
FÜR BIOPHYSIK

MPI für Biophysik · Max-von-Laue-Straße, 3 · 60438 Frankfurt am Main

Mr. Cristian Parra

Magdalena Kose
Personalstelle
Tel.: +49 (0) 69 6303 - 4503
Fax: +49 (0) 69 6303 - 4502
makose@biophys.mpg.de
#: *mk/2023*

19. Juli 2023

Arbeitsbescheinigung / Confirmation

Sehr geehrte Damen und Herren,

Hiermit bestätigen wir, dass Cristian Alirio Parra Jimenez, geboren am 31.01.1994, in der Abteilung „Theoretische Biophysik" von Herrn Prof. Dr. Gerhard Hummer circa 3 Monate in Rahmen eines freiwilligen Praktikums tätig war unter der Beaufsichtigung von Dr. Sergio Cruz. Die Max-Planck-Gesellschaft zur Förderung der Wissenschaften ist ein eingetragener Verein (Vereinsregister AG Berlin-Charlottenburg, Nr.: VR 13378Nz) und wird zu über 90% aus öffentlichen Mitteln des Bundes und der Länder finanziert. Das Max-Planck-Institut für Biophysik ist ein rechtlich unselbständiges Institut dieser Gesellschaft.

Herewith we want to confirm, that Mr. Cristian Alirio Parra Jimenez, born on 31.01.1994, made a voluntary Internship for 3 months in the group "Theoretical Biophysics" directed by Prof. Dr. Gerhard Hummer under the supervision of the post-doc from the same group, Dr. Sergio Cruz.
The Max Planck Society for the Advancement of Science is a registered association (Vereinsregister AG Berlin-Charlottenburg, Nr.: VR 13378Nz) and is financed to over 90% by public funds from the federal and state governments. The Max Planck Institute for Biophysics is a legally dependent institute of this society.

Max-Planck-Institut
für Biophysik
Max-von-Laue-Straße 3
D-60438 Frankfurt

i. A.

Magdalena Kose
Sachgebietsleiterin Personal / HR Manager

Max-Planck-Institut für Biophysik
Max-von-Laue-Straße 3
60438 Frankfurt am Main

Tel.: + 49 (0) 69 6303 - 4503

magdalena.kose@biophys.mpg.de
www.biophys.mpg.de

Medellín
SUQUI 2022
3er Simposio Universitario de Investigación en Química

Medellín, Colombia
Septiembre 14 al 16 de 2022

Universidad® de Medellín
Ciencia y Libertad

El comité organizador de 3er Simposio Universitario de Investigación en Química (3er SUQUI) **certifica** que

Cristian Alirio Parra Jimenez

participó en el evento con el cartel titulado

"A Toy Model for the Crystalizacion Process of the Malaria Pigment Hemozoin "

Fco Núñez Zarur

Francisco Núñez Zarur
Presidente
Comité Organizador 3er Suqui

José Alberto Rúa Vásquez

José Alberto Rúa
Decano
Facultad de Ciencias Básicas
Universidad de Medellín

Armenia, septiembre 28 de 2022

EL DIRECTOR DEL XXIX CONGRESO NACIONAL DE FÍSICA

CERTIFICA QUE EL TRABAJO TITULADO

A toy model for the crystallization process of the Malaria pigment Hemozoin

fue presentado por ***Cristian Alirio Parra Jimenez, Olga Lopez-Acevedo*** en el marco del XXIX Congreso Nacional de Física realizado en la Universidad del Quindío de la ciudad de Armenia, del 21 al 23 de septiembre de 2022.

HERNANDO ARIZA CALDERÓN
Director
XXIX Congreso Nacional de Física

B

Codes Used in this Work

Here we present the codes used in this work, starting with the calculators used to obtain the fits for the experimental kinetic data, followed by the codes used to simulate the IR spectra and finishing with the cellular automaton.

```
import numpy as np

import matplotlib.pyplot as plt

import pandas as pd

from scipy import optimize

from ipywidgets import interact

from tqdm import tqdm

from ipywidgets import FloatSlider, fixed


######################

####### MODELS #######

######################


# Pasternack Model


def lin_exp(t,y2,ks):

    return y2-y2*np.exp(-ks*t)


def avrami(t,y1,n,k):

    return (y1-y1*np.exp(-k*t**n))


def y_Pasternack_2(t,y0,y1,y2,n,k,ks):

    return y0-y1*np.exp(-((k)*(t)**(n)))-y2*np.exp(-ks*t)


# Second order Model
```

```
def r_sec_mod(t,a,k):
    # Corrected dimer form model
    return a - a / (a*k*t + 1)

def r_growth(t,b,k,D):
    # Corrected Avrami model
    return  b/ (1 + np.exp(-b*k*t + D))

def r_nuc_gro(t,a,k1,b,k2,D):
    return r_sec_mod(t,a,k1) + r_growth(t,b,k2,D)

############################
####### Functions ##########
############################

def paramt_cal(times,values,fun,poss=None,bounds= (-np.inf, np.inf),sigma= None):

    t = times
    y_exp = values
    guess = poss
    popt, pcov = optimize.curve_fit(fun,t,y_exp,bounds=bounds,p0=guess,
                                    sigma=sigma,method='trf',maxfev=5000)
    return popt
```

```
def cov_cal(times,values,fun,poss=None,bounds= (-np.inf, np.inf),sigma= None ):

    t = times
    y_exp = values
    guess = poss
    popt, pcov = optimize.curve_fit(fun,t,y_exp,bounds=bounds,p0=guess,
                                    sigma=sigma ,method='trf',maxfev=5000)
    return pcov



def varia_parm_cal(times,values,fun,poss=None,bounds= (-np.inf, np.inf),sigma= None):
    return np.sqrt(np.diag(cov_cal(times,values,fun,poss=poss,bounds= bounds,sigma= sigma)))



def errors(times,values,fun,poss=None,bounds= (-np.inf, np.inf),sigma= None):

    param = paramt_cal(times,values,fun,poss=poss,bounds= bounds,sigma= sigma)
    t = times
    n = len (t)
    y_exp = values
    y_mexp = np.mean(y_exp)
    y_calc = fun(t,*param)

    ssr = np.sum (np.array([ (y_exp[i] -y_calc[i])**2 for i in range (len(t))]))
    sst = np.sum(np.array([(y_exp[i] - y_mexp)**2 for i in range(len(t))]))
```

```
    rmse = np.sqrt(ssr/n)
    rr = 1 - ssr/sst
    MAPE =  (np.array([np.abs(y_exp[i] - y_calc[i])/np.abs(y_exp[i]) for i in range(1,len(t))]))
    MAPE = (100/len(t))* np.sum(MAPE)

    return f"""R² = {rr.round(4)}, RMSE = {rmse.round(4)}, MAPE = {MAPE.round(4)} \n
    {rr.round(4)} & {rmse.round(4)} & {MAPE.round(4)}"""

def MAPE_calc(times,values,fun,poss=None,bounds= (-np.inf, np.inf),sigma= None):
    param = paramt_cal(times,values,fun,poss=poss,bounds= bounds,sigma= sigma)
    t = times
    n = len (t)
    y_exp = values
    y_mexp = np.mean(y_exp)
    y_calc = fun(t,*param)
    MAPE =  (np.array([np.abs(y_exp[i] - y_calc[i])/np.abs(y_exp[i]) for i in range (len(t)) ]))
    MAPE = (100/len(t))* np.sum(MAPE)
    return MAPE

def graph(times,values,fun,popt,label,drug,color="tomato"):

    t = times
    n = len (t)
    y_exp = values
```

```
    plt.plot(t,y_exp,'s',markersize=5.5,color="black",
            label=r"$\beta$-Hem Aq Med" "\n" f"+ {drug}")
    plt.plot(t,fun(t,*popt),linewidth = 1.5, color=f"{color}",label= f"{label}")
    plt.legend(loc='lower right',fontsize = 8)
    plt.xlabel(r" t (h)")
    plt.ylabel(" Y %  of Convertion")
    plt.ylim(0,100)
    plt.yticks(np.arange(0, 101, 10))
    plt.title(f" {label} + {drug} ")
    plt.grid()
    plt.show()
    # plt.savefig(f"{label}_{drug}.jpg")

def cov_graph(times,values,fun,poss=None,label=" ",drug=" ",bounds= (-np.inf, np.inf),sigma=None):

    covi = cov_cal(times, values, fun,bounds= bounds,poss=poss,sigma=sigma)
    plt.imshow(np.log(np.abs(covi)))
    plt.colorbar()
    plt.title(f"Cov M {label}+{drug} ")
    plt.show()
    # plt.savefig(f"{label}_{drug}.jpg")

def resum_maker(medium, times,values,fun,label,drug,color="tomato",
                poss=None,bounds= (-np.inf, np.inf),sigma= None):
```

```
s = paramt_cal(times,values,fun,poss=poss,bounds= bounds,sigma=sigma).round(4)

s_len = len (s)

delta_s = varia_parm_cal(times,values,fun,poss=poss,bounds= bounds,sigma=sigma).round(4)


if s_len == 6:

    y0,y1, y2, n, k, ks= s

    da,dy1, dy2, dn, dk, dks = delta_s

    print (" y0 = {}, y1 = {}, y2 = {}, n = {}, k = {}, ks = {}".format(*s))

    print ("\u0394y0 = {}, \u0394y1 = {}, \u0394y2 = {},

            \u0394n = {}, \u0394k = {}, \u0394ks = {}".format(*delta_s))

    print ("################################")

    print (f"y0 = {y0} ({da}), y1 = {y1} ({dy1}), y2 = {y2} ({dy2}),

            n = {n} ({dn}), k = {k} ({dk}), ks = {ks} ({dks})")

    print (f"{y0}$\pm$({da})&{y1}$\pm$({dy1})&{y2}$\pm$({dy2})

            &{n}$\pm$({dn})&{k}$\pm$({dk})&{ks}$\pm$ ({dks})")


else:

    a,k1,b,k2,D = s

    da,dk1,db,dk2,dD = delta_s

    print (" a = {}, k1 = {}, b = {}, k2 = {}, D = {}".format(*s))

    print ("\u0394a = {}, \u0394k1 = {}, \u0394b = {},

            \u0394k2 = {}, \u0394D = {}".format(*delta_s))

    print ("################################")

    print (f"a = {a} ({da}), k1 = {k1} ({dk1}), b = {b} ({db}),

            k2 = {k2} ({dk2}), D = {D} ({dD})")
```

```
        print (f"{a}$\pm$({da})&{k1}$\pm$({dk1})&{b}$\pm$({db})
                &{k2}$\pm$({dk2})&{D}$\pm$({dD})")

    print (errors(times,values,fun,poss=poss,bounds= bounds,sigma=sigma))
    cov_graph(times,values,fun,poss=poss,label=label,drug=drug,bounds= bounds,sigma=sigma)
    graph(times,values,fun,s,f"""{label}""",f"""{drug}""",f"""{color}""")

    if medium == "oil" and s_len == 6:
        oil_parts_pasternack(times,values,lin_exp,avrami,y_Pasternack_2,sigma,bounds,poss)

    elif medium == "oil" and s_len == 5:
        oil_parts_sec_mod_rev(times,values,r_sec_mod,r_growth,r_nuc_gro,sigma,bounds,poss)

    elif medium == "aqua" and s_len == 6:
        aqueous_parts_pasternack(times,values,lin_exp,avrami,y_Pasternack_2,sigma,bounds,poss)

    elif medium == "aqua" and s_len == 5:
        aqueous_parts_sec_mod_rev(times,values,r_sec_mod,r_growth,r_nuc_gro,sigma,bounds,poss)

    else:
        raise ValueError("The Medium or the number of parameters is not correct")

##############################################
####### Aqueous  Parameters ##################
##############################################
```

```
def aqueous_parts_pasternack(t,data,model_1,model_2,combined_model,sigma,bounds,poss,alpha=0.5):
    tt = np.linspace(0, 4, 200)
    y0,y1,y2,n,k,ks = paramt_cal(t,data,combined_model,poss=poss,bounds= bounds,sigma=sigma).round(4)
    print (f" y0 = {y0}, y1 = {y1}, y2 = {y2}, n = {n}, k[1/h] = {k}, ks[1/h] = {ks}")
    plt.plot(tt,model_1(tt,y2,ks),label="Lin Exp")
    plt.plot(tt,model_2(tt,y1,n,k),label="Avrami")
    plt.plot(tt,combined_model(tt,y0,y1,y2,n,k,ks),label="Pasternack", alpha=alpha)

    plt.plot(t, data,'s',markersize=5.5,color="black",label=r"Exp Data ")
    plt.errorbar(t, data,yerr=sigma,fmt='s',color="black")
    plt.legend(loc='lower right',fontsize = 8)
    plt.xlabel(r" t (h)")
    plt.ylabel(" Y %  of Convertion")
    plt.grid()
    plt.show()
    print (f" y0 = {y0}, y1 = {y1}, y2 = {y2}, n = {n}, k[1/h] = {k}, ks[1/h] = {ks}")

def aqueous_parts_sec_mod_rev(t,data,model_1,model_2,combined_model, sigma,bounds, poss,alpha=0.5):
    tt = np.linspace(0, 4, 200)
    a,k1,b,k2,D = paramt_cal(t,data,combined_model,poss=poss,bounds= bounds,sigma=sigma).round(4)
    print (f"a={a},k1={k1},b={b},k2={k2},D={D}")
    plt.plot(tt,model_1(tt,a,k1),label="Dim Form")
    plt.plot(tt,model_2(tt,b,k2,D),label="Logistic")
    plt.plot(tt,combined_model(tt,a,k1,b,k2,D),label="Sec Ord",alpha=alpha)
```

```
    plt.plot(t,data,'s',markersize=5.5,color="black",label=r"Exp Data ")
    plt.errorbar(t,data,yerr=sigma,fmt='s',color="black")
    plt.legend(loc='lower right',fontsize = 8)
    plt.xlabel(r" t(h)")
    plt.ylabel(" Y %  of Convertion")
    plt.grid()
    plt.show()
    print (f"a={a},k1={k1},b={b},k2={k2},D={D}")

def aqueous_explorer_Pasternack(t,y_exp,y0, y1, y2, n, k, ks,alph=0.5):
    tt = np.linspace(0, 4, 100)

    plt.plot(tt,lin_exp(tt,y2, ks),label="Dim Form ")
    plt.plot(tt,avrami(tt,y1,n, k),label="Logistic")
    plt.plot(tt,y_Pasternack_2(tt,y0, y1, y2, n, k, ks),label="Sec Ord",alpha=alph)
    plt.plot(t,y_exp,'s',markersize=5.5,color="black",label=r"Exp Data ")
    plt.xlabel(r" t(h)")
    plt.ylabel(" Y %  of Convertion")
    plt.legend()
    plt.grid()
    plt.show()

def aqueous_explorer_RSM(t,y_exp,a,k1,b,k2,D,alph=0.5):
    tt = np.linspace(0, 4, 100)
```

```
    plt.plot(tt,r_sec_mod(tt,a,k1),label="Dim Form ")
    plt.plot(tt,r_growth(tt,b,k2,D),label="Logistic")
    plt.plot(tt,r_nuc_gro(tt,a,k1,b,k2,D),label="Sec Ord",alpha=alph)
    plt.plot(t,y_exp,'s',markersize=5.5,color="black",label=r"Exp Data ")
    plt.xlabel(r" t (h)")
    plt.ylabel(" Y %  of Convertion")
    plt.legend()
    plt.grid()
    plt.show()

##############################################
####### Oil Parameters ######################
##############################################

def oil_parts_pasternack(t,data,model_1,model_2,combined_model,sigma,bounds,poss):
    tt = np.linspace(0, 100, 200)
    y0,y1,y2,n,k,ks = paramt_cal(t,data,combined_model,poss=poss,bounds= bounds,sigma=sigma).round(4)
    print (f" y0 = {y0}, y1 = {y1}, y2 = {y2}, n = {n}, k[1/m] = {k}, ks[1/m] = {ks}")
    plt.plot(tt,model_1(tt,y2,ks),label="Lin Exp")
    plt.plot(tt,model_2(tt,y1,n,k),label="Avrami")
    plt.plot(tt,combined_model(tt,y0,y1,y2,n,k,ks),label="Pasternack", alpha=0.5)

    plt.plot(t, data,'s',markersize=5.5,color="black",label=r"Exp Data ")
    plt.errorbar(t, data,yerr=sigma,fmt='s',color="black")
```

```
    plt.legend(loc='lower right',fontsize = 8)
    plt.xlabel(r" t(m)")
    plt.ylabel(" Y %  of Convertion")
    plt.yticks(np.arange(0, 101, 10))
    plt.grid()
    plt.show()
    print (f" y0 = {y0}, y1 = {y1}, y2 = {y2}, n = {n}, k[1/m] = {k}, ks[1/m] = {ks}")


def oil_parts_sec_mod_rev(t,data,model_1,model_2,combined_model,
                          sigma,bounds=(-np.inf, np.inf), poss=None,alpha=0.5):
    tt = np.linspace(0, 100, 200)
    a,k1,b,k2,D = paramt_cal(t,data,combined_model,poss=poss,bounds= bounds,sigma=sigma).round(4)
    print (f"a={a},k1={k1},b={b},k2={k2},D={D}")
    plt.plot(tt,model_1(tt,a,k1),label="Dim Form",alpha=alpha)
    plt.plot(tt,model_2(tt,b,k2,D),label="Logistic",alpha=alpha)
    plt.plot(tt,combined_model(tt,a,k1,b,k2,D),label="Sec Ord")

    plt.plot(t,data,'s',markersize=5.5,color="black",label=r"Exp Data ")
    plt.errorbar(t,data,yerr=sigma,fmt='s',color="black")
    plt.legend(loc='lower right',fontsize = 8)
    plt.xlabel(r" t(m)")
    plt.ylabel(" Y %  of Convertion")
    plt.yticks(np.arange(0, 101, 10))
    plt.grid()
    plt.show()
```

```
    print (f"a={a},k1={k1},b={b},k2={k2},D={D}")


def oil_explorer_Pasternack(t,y_exp,y0, y1, y2, n, k, ks,alph=0.5):
    tt = np.linspace(0, 100, 200)
    plt.plot(tt,lin_exp(tt,y2, ks),label="Dim Form ")
    plt.plot(tt,avrami(tt,y1,n, k),label="Logistic")
    plt.plot(tt,y_Pasternack_2(tt,y0, y1, y2, n, k, ks),label="Sec Ord",alpha=alph)
    plt.plot(t,y_exp,'s',markersize=5.5,color="black",label=r"Exp Data ")
    plt.xlabel(r" t(m)")
    plt.ylabel(" Y %  of Convertion")
    plt.yticks(np.arange(0, 101, 10))
    plt.legend()
    plt.grid()
    plt.show()


def oil_explorer_RSM(t,y_exp,a,k1,b,k2,D,alph=0.5):
    tt = np.linspace(0, 100, 200)


    plt.plot(tt,r_sec_mod(tt,a,k1),label="Dim Form ")
    plt.plot(tt,r_growth(tt,b,k2,D),label="Logistic")
    plt.plot(tt,r_nuc_gro(tt,a,k1,b,k2,D),label="Sec Ord",alpha=alph)
    plt.plot(t,y_exp,'s',markersize=5.5,color="black",label=r"Exp Data ")
    plt.xlabel(r" t (m)")
    plt.ylabel(" Y %  of Convertion")
    plt.yticks(np.arange(0, 101, 10))
```

```
    plt.legend()
    plt.grid()
    plt.show()
```

Simulated IR Spectra.

```
###### Geometry Optimization
from ase import Atoms
from ase.io import read
from gpaw import GPAW, restart
from gpaw import Mixer, MixerSum, MixerDif
from ase.calculators.vdwcorrection import vdWTkatchenko09prl
from gpaw.analyse.hirshfeld import HirshfeldPartitioning
from gpaw.analyse.vdwradii import vdWradii

h=0.18
atoms = read("second.xyz")

c = GPAW(mode='fd',
           h=h,
           xc="PBE",
           spinpol=True,
           nbands=-10,
           convergence={'energy': 0.0001},
```

```
            txt = "out.txt",
            mixer=MixerSum(0.02, 5, 100),
            #eigensolver=Davidson(4),
            #parallel={"sl_auto":True},
        #hund=True,
            maxiter=900,
            #charge=0
            )

calc = vdWTkatchenko09prl(HirshfeldPartitioning(c),
        vdWradii(atoms.get_chemical_symbols(), 'PBE'))

atoms.calc = calc

e = atoms.get_potential_energy()

from ase.vibrations import Infrared
ir = Infrared(atoms)
ir.run()
ir.summary(log='vib_summary.log')

######## IR Spectra

#run from serial
from ase import Atoms
```

```
from ase.io import read
from gpaw import GPAW, restart

h=0.18
atoms = read("second.xyz")

from ase.vibrations import Infrared
ir = Infrared(atoms)
ir.run()
#write ir-spectra.dat
ir.write_spectra(width=1)

#write ir.mode.traj
#list_modes =[443,442,441,395,393,392,390,389,387,385,384,383,382,381,380,377,
                376,375,374,355,354,353,352,341,314,303,302,301,299,294,
                293,290,288,287,286,285,284,283,281,270,268,267,266,264,
                260,249,248,247,246,245,244]
list_modes =[]
for i in range(382,444):
    list_modes.append(i)

for i in list_modes:
ir.write_mode(i, kT=0.1)

######### IR Summary
```

```
from ase import Atoms

from ase.io import read

from gpaw import GPAW, restart

from gpaw import Mixer, MixerSum, MixerDif

from ase.calculators.vdwcorrection import vdWTkatchenko09prl

from gpaw.analyse.hirshfeld import HirshfeldPartitioning

from gpaw.analyse.vdwradii import vdWradii

from ase.vibrations import Infrared


h=0.18

atoms = read("second.xyz")


ir = Infrared(atoms)

ir.run()

ir.summary(log='vib_summary.log')


############ Vibration analizer


## Parametrization of the Dimer


metilos = {'m1': [(58,64),(58,65),(58,66)],

           'm2': [(57,1),(57,4),(57,63)],

           'm3': [(22,18),(22,28),(22,29)],

           'm4': [(19,13),(19,16),(19,25)],
```

```
            'm5': [(95,91),(95,101),(95,102)],
            'm6': [(130,74),(130,77),(130,136)],
            'm7': [(132,137),(132,138),(132,139)],
            'm8': [(92,86),(92,89),(92,98)]}

vinilos = {'v1': [(62,56),(62,69),(62,70),(70,72),(70,71)],
           'v2': [(55,48),(55,60),(55,61),(61,68),(61,67)],
           'v3': [(135,129),(135,143),(135,142),(142,144),(142,145)],
           'v4': [(128,121),(128,134),(128,133),(133,140),(133,141)]}

chain_fe = {'chain_1': [(39,27),(39,43),(39,42),(39,37),(37,32),
                        (37,34),(37,45),(45,52),(45,44),(44,147)],
            'chain_2': [(112,100),(112,115),(112,116),(112,110),(110,105),
                        (110,107),(110,118),(118,125),(118,117),(117,146)]}

chain_no_fe = {'chain_no-Fe_1': [(108,96),(108,113),(108,109),(108,104),(104,103),
                                 (104,97),(104,114),(114,119),(114,111),(111,124)],

               'chain_no-Fe_2': [(35,23),(35,40),(35,36),(35,31),(31,30),
                                 (31,24),(31,41),(41,46),(41,38),(38,51)]}
nitrogens = {'N1': [(146,12),(12,11),(12,0),(146,15),(15,21),(15,14),
                    (146,5),(5,6),(5,49),(146,2),(2,3),(2,47)],

             'N2': [(147,78),(78,122),(78,79),(147,88),(88,87),(88,94),
                    (147,85),(85,73),(85,84),(147,75),(75,120),(75,76)]}
```

```
porphyrin = {"porfirin_1" : [(0,26),(26,33),(26,21),(21,27),(27,20),(20,14),(14,9),
                             (9,10),(9,6),(6,50),(50,56),(56,49),(49,54),(54,59),(54,47),
                             (47,53),(53,48),(48,3),(3,8),(8,7),(8,11),(11,17),(17,23),(23,0)],
             "porfirin_2" : [(122,129),(129,123),(123,79),(79,82),(82,83),(82,87),(87,93),
                             (93,100),(100,94),(94,99),(99,106),(99,73),(73,96),(96,90),(90,84),
                             (84,81),(81,80),(81,76),(76,121),(121,127),(127,120),(120,126),(126,131),
                             (126,122)]}

Fe_Fe = {'Fe-Fe': [(146,147)]} # hierro - hierro

Fe_OO_CC = {'C=O-(Fe)_1': [(118,125)], # Enlace C=O asociado a pico 1664
            'C=O-(Fe)_2': [(45,52)]}

Fe_O_C = {'C-O-Fe_1': [(118,117),(117,146)], # ENlace Fe-O-C pico de 1200
          'C-O-Fe_2': [(45,44),(44,147)]}

H_O_C = {'H_O_C_1': [(114,111),(111,124)],
         'H_O_C_2': [(41,38),(38,51)]} # pico asociado al enlace entre dimeros

No_Fe_OO_CC = {'C=O_1': [(114,119)], # pico asociado a los C=O que no tienen un hierro
               'C=O_2': [(41,46)]}

iron_bonds = {"Fe_N1" : [(146,12),(146,15),(146,5),(146,2)],
              "Fe_O1" :[(117,146)] ,
```

```
            "Fe_N2": [(147,78),(147,88),(147,85),(147,75)],
            "Fe_O2" : [(44,147)]}

############
#### Function to check the bonds of the specific dictionaries
def resumen_per_fun_grup_specific_traj(fun_grup):

    llaves = nom_molec(fun_grup)
    contador = number_bonds(fun_grup,llaves)
    molecules_and_bonds = keys_bonds_list(fun_grup)
    num_traj = 245
    total_num_bonds= len(molecules_and_bonds)
    follow_list_frame = []
    data = []
    for mol in range (total_num_bonds):

        nom = molecules_and_bonds[mol][0]
        direcc = molecules_and_bonds[mol][1]
        i,j = direcc[0], direcc[1]
        frame, percent = max_dist_frame(num_traj, i, j)

        #print (molecules_and_bonds[mol],type (molecules_and_bonds[mol]),nom,i,j,frame,percent)
        row = {"molecule":nom, "atom bond": (i,j), "max frame" : frame, "max sep %": percent}
        data.append(row)
        """ sigue poner una funcion que me encuentre la separacion maxima d -do y me saque el frame
```

```
        asociado a eso --> max_dist_frame(num,i,j)"""
        follow_list_frame.append ((nom,direcc,frame,percent))

    a = pd.DataFrame(data)
    return a
resumen_per_fun_grup_specific_traj(metilos)
```

Cellular Automaton.

```
import pygame
import pygame.time
import numpy as np
import matplotlib.pyplot as plt

class Grid:

    def __init__(self,width,height,scale,density,cloroquine,offset,stop):

        """
        creates a unique array which is filled with a
        specific number of ones given by the entry density.

        the number of entries in the array are given by
        the width and height parameters and the
```

```
    """


    self.scale = scale
    self.density = density
    self.cloroquine = cloroquine


    self.rows = int (width / scale )
    self.columns = int (height / scale)


    self.size = (self.rows, self.columns)
    self.grid1_array = np.array([0] * (self.size[0] * self.size[1] - self.density - self.cloroquine)
                        [1]*self.density + [2]*self.cloroquine)
    np.random.shuffle(self.grid1_array)
    self.grid1_array.shape = self.size
    self.offset = offset
    self.stop = stop


def Conway(self,off_color, on_color,on_cloro ,surface,critical, pause,breaker):


    """
    takes every possition in the array and assign to it a
    an on_color for the ones and a off_color for the zeros
    and paints them in a pygame surface.


    """
```

```
for x in range (self.rows):
    for y in range(self.columns):
        x_pos = x * self.scale
        y_pos = y * self.scale

        if self.grid1_array[x][y] == 1:
            pygame.draw.rect(surface, on_color,[x_pos, y_pos, self.scale - self.offset,
                            self.scale - self.offset ])
        elif self.grid1_array[x][y] == 2:
            pygame.draw.rect(surface, on_cloro,[x_pos, y_pos, self.scale - self.offset,
                            self.scale - self.offset ])
        else :
            pygame.draw.rect(surface, off_color,[x_pos, y_pos, self.scale - self.offset,
                                self.scale - self.offset ] )

"""
the next step is put the dinamycs of the system
where the number of on neighbours gives the square
stability or is dissolved and move around randomly
"""
next = np.ndarray(shape = (self.size))
zeros = []
if pause == False:
    "counter of crystallized molecules"
    keep = int(0)
```

```
”counter of cloroquine particles”
quina = int(0)


for x in range (self.rows):
    for y in range(self.columns):
        state = self.grid1_array[x][y]
        neighbours, posi = self.get_neighbours(x,y)[0], self.get_neighbours(x,y)[1]


        if state == 1 and (neighbours >= critical):
            next[x][y] = 1
            keep += 1


        elif state == 1 and (neighbours < critical) :
            next[x][y] = 0
            zeros.append((x,y))


        elif state == 2 and ((neighbours == 0)):
            next[x][y] = 0
            zeros.append((x,y))
            quina += 1


        elif state == 2 and (neighbours >= 1):
            next[posi[0][0]][posi[0][1]] = 0
            next[x][y] = 0
            self.density -= 1
```

```
            self.cloroquine -= 1


        else :
            next[x][y] = state
            if state == 0:
                zeros.append((x,y))


crystal = (keep/self.density)
print (crystal)
particles = next.sum() -int(self.cloroquine) * 2
carencia = int (self.density - particles)
np.random.shuffle(zeros)


graber_1 = zeros [:carencia]


for carente in range (carencia):
    next[graber_1[carente][0]][graber_1[carente][1]] = 1


zeros = [i for i in zeros if i not in graber_1]


quino_grab = zeros[:quina]
for qui in quino_grab:
    next[qui[0]][qui[1]] = 2


if keep >= int (self.stop * self.density):
```

```
            breaker = False
            return breaker, crystal
        else:
                self.grid1_array = next
                breaker = True
                return breaker, crystal

# def get_neighbours(self, x, y):

#     """
#     counts the number of ones and zeros around every point
#     in the grid array (which is filled with ones and zeros)
#     and returns the number of ones around every point.
#     """
#     total = 0
#     for n in range (-1, 2):
#         for m in range(-1,2):
#             x_edge = (x+n+self.rows) % self.rows
#             y_edge = (y+m+self.columns) % self.columns
#             total += self.grid1_array[x_edge][y_edge]
#     total -= self.grid1_array[x][y]
#     return total

def get_neighbours(self, x, y):
    "counts the number of ones and zeros around every pointin the grid array"
```

```
    total = 0
    pair = []
    for n in range (-1, 2):
        for m in range(-1,2):
            ”search perimeter of x,y possition”
            x_edge = (x+n+self.rows) % self.rows
            y_edge = (y+m+self.columns) % self.columns
            if self.grid1_array[x_edge][y_edge] == 1 :
                ”locate the ones”
                if (x_edge,y_edge) == (x,y):
                    ”exclude the center possition (do not count yourself)”
                    total += 0
                else :
                    ”sum the rest and grab the possition of the ones”
                    total += self.grid1_array[x_edge][y_edge]
                    pair.append((x_edge,y_edge))
            else:
                ”ignore the 0s and the 2s”
                total += 0
    np.random.shuffle(pair)
    ”total of ones around (x,y) and the possition of a one ”
    return total, pair


# def get_neighbours(self, x, y):
```

```
#     """
#     Modified selection rule for neighbours in the centers
#     """
#     total = 0
#     for n in range (-1, 2):


#         if n == -1:
#             m = 0
#             x_edge = (x+n+self.rows) % self.rows
#             y_edge = (y+m+self.columns) % self.columns
#             total += self.grid1_array[x_edge][y_edge]


#         elif n == 0:
#             for m in range(-1,2):
#                 x_edge = (x+n+self.rows) % self.rows
#                 y_edge = (y+m+self.columns) % self.columns
#                 total += self.grid1_array[x_edge][y_edge]
#         elif n == 1:
#             m = 0
#             x_edge = (x+n+self.rows) % self.rows
#             y_edge = (y+m+self.columns) % self.columns
#             total += self.grid1_array[x_edge][y_edge]


#     total -= self.grid1_array[x][y]
#     return total
```

```
# def get_neighbours(self, x, y):

#     """
#      Modified selection rule for neighbours in the diagonals
#     """
#     total = 0
#     for n in range (-1, 2):

#         if n == -1:
#             mes = [-1,1]
#             for m in mes :
#                 x_edge = (x+n+self.rows) % self.rows
#                 y_edge = (y+m+self.columns) % self.columns
#                 total += self.grid1_array[x_edge][y_edge]

#         elif n == 0:
#             m = 0
#             x_edge = (x+n+self.rows) % self.rows
#             y_edge = (y+m+self.columns) % self.columns
#             total += self.grid1_array[x_edge][y_edge]

#         elif n == 1:
#             mes = [-1,1]
#             for m in mes :
```

```
    #                 x_edge = (x+n+self.rows) % self.rows
    #                 y_edge = (y+m+self.columns) % self.columns
    #                 total += self.grid1_array[x_edge][y_edge]

    #     total -= self.grid1_array[x][y]
    #     return total

width, height = 1200, 900
size = (width, height)
scale = 10
offset = 1

pygame.init()
pygame.display.set_caption("Molecules")
screen = pygame.display.set_mode(size)

fps = 60

time = 0

black = (0,0,0)
blue = (0,121,150)
verde = (0,255,0)
white = (255,255,255)
```

```
stop = 1

sigma = 0.16


concentration = 0.2 * np.exp(sigma)


critical =  int ((2 * (0.708 * 10 ** -27) * (23 * 10 ** -3)  /

                ((sigma )* 310.15 * 1.38 * 10 ** -23 ) ) * 10 ** 8)

print ( " El radio critico viene dado por {}".format(critical))


#density = int (concentration *(width * height) / (scale * scale ))

density =   int(0.26 * ( (width * height) / (scale * scale )))

cloroquine = int (0.0*density)


print (f" la densidad del sistema es {density} con un discriminante de {int (0.5 * 0.01 * density) }

        y {int ( 0.05 * density) } no cristalizadas")


grid = Grid(width,height,scale,density,cloroquine,offset,stop)


pause = False

run = True

itero = 0

crist = []


while run:

    itero += 1
```

```
    clock = pygame.time.Clock()
    clock.tick(fps)
    time = pygame.time.get_ticks() / 1000
    screen.fill(black)

    breaker = grid.Conway(off_color=white, on_color=blue,on_cloro=verde,
                surface=screen,critical=critical, pause = pause,breaker= run)

    crist.append(breaker[1])
    breaker = breaker[0]

    if breaker == False:
        run = False
    else :
        run = True
        for event in pygame.event.get():
            if event.type == pygame.QUIT:
                run = False
            if event.type == pygame.KEYUP:
                if event.key == pygame.K_ESCAPE:
                    run = False
                if event.key == pygame.K_SPACE:
                    pause = not pause
        pygame.display.update()
pygame.quit()
```

```
print (”\n” f”a una concentracion de {concentration * 100}% el sistema tarda {itero}
            iteraciones en nuclear con un radio critico de {critical} vecinos”)
```

C

Derivation of the Second Order Crystallization Model

In this section, we present the derivation of the second order model of crystallization. The starting point is the second order term, associated with the dimer formation process.

C.0.1 Dimer Formation

We start with the following differential equation:

$$\frac{dY}{dt} = k_1 (\alpha - Y)^2 \tag{C.1}$$

Doing separation of variables, we obtain:

$$\frac{dY}{(\alpha - Y)^2} = k_1 dt$$

Integrating in both sides:

$$\int \frac{dY}{(\alpha - Y)^2} = \int_0^t k_1 \, dt$$

$$-\int \frac{d(\alpha - Y)}{(\alpha - Y)^2} = k_1 \, t + C$$

$$\frac{1}{(\alpha - Y)} = k_1 \, t + C$$

$$\frac{1}{k_1 \, t + C} = \alpha - Y$$

$$Y = \alpha - \frac{1}{k_1 \, t + C}$$

for $t = 0$, the number of dimers formed must be zero, meaning that $Y(t = 0) = 0$. Plugging this value in the equation, we obtain:

$$Y = \alpha - \frac{1}{C} = 0 \ \rightarrow C = \frac{1}{\alpha}$$

and finally obtaining:

$$Y = \alpha - \frac{\alpha}{\alpha\, k_1\, t + 1} \tag{C.2}$$

C.0.2 Crystallization Process

In this section, we derive the equation used to represent the crystallization process in the SOM. We used a logistic function as a starting point for our differential equation:

$$\frac{dY}{dt} = k_2\, Y(\beta - Y) \tag{C.3}$$

We use separation of variables between the Crystallization term (Y) and time.

$$\frac{dY}{Y(\beta - Y)} = k_2\, dt$$

We notice that the left-hand side (LHS) of the equation can be expressed as partial sums. This will simplify our work when we need to integrate, with respect to the total yield of crystallized material.

$$\frac{1}{Y(\beta - Y)} = \frac{A}{Y} + \frac{B}{(\beta - Y)}$$

We know that this must be an identity for all values of Y. So in the numerator we have the following equation.

$$A\,(\beta - Y) + B\,Y = 1$$

Re-arranging the terms we obtain.

$$A\,\beta + Y(B - A) = 1 \rightarrow A = B$$

where $A = \frac{1}{\beta}$

which implies:

$$\frac{1}{\beta\, Y} + \frac{1}{\beta(\beta - Y)} = \frac{1}{Y(\beta - Y)}$$

Now, integrating in both sides.

$$\int dY \frac{1}{Y(\beta - Y)} = \int dY \left(\frac{1}{\beta\, Y} + \frac{1}{\beta(\beta - Y)} \right) = \int_0^t k_2\, dt$$

$$\ln\left(\frac{Y}{\beta - Y} \right) = \beta\, k_2\, t + C$$

$$\frac{Y}{\beta - Y} = \exp(\beta\, k_2\, t + D)$$

After separating, Y we obtain:

$$Y = \frac{\beta}{1 + \exp\{-(\beta\, k_2\, t + D)\}} \tag{C.4}$$

Adding Equations C.2 and C.4, we obtain the crystallization model shown in Chapter 1.

$$Y = \alpha - \frac{\alpha}{\alpha\, k_1\, t + 1} + \frac{\beta}{1 + \exp\{-(\beta\, k_2\, t + D)\}} \tag{C.5}$$

D

Fair Use of Graphs

In this academic work, we used one graph from the paper *On the kinetics of formation of hemozoin, the malaria pigment*[1]. Here, we present the written permission given to use to make use of them in Section 3

ELSEVIER LICENSE
TERMS AND CONDITIONS

Feb 06, 2024

This Agreement between Universidad de AntioquiA -- Cristian Parra Jimenez ("You") and Elsevier ("Elsevier") consists of your license details and the terms and conditions provided by Elsevier and Copyright Clearance Center.

License Number	5723241478496
License date	Feb 06, 2024
Licensed Content Publisher	Elsevier
Licensed Content Publication	Journal of Inorganic Biochemistry
Licensed Content Title	On the kinetics of formation of hemozoin, the malaria pigment
Licensed Content Author	Robert F. Pasternack,Ben Munda,Abigail Bickford,Esther J. Gibbs,Luigi Monsù Scolaro
Licensed Content Date	Oct 1, 2010
Licensed Content Volume	104
Licensed Content Issue	10
Licensed Content Pages	6
Start Page	1119
End Page	1124

Type of Use	reuse in a thesis/dissertation
Portion	figures/tables/illustrations
Number of figures/tables/illustrations	2
Format	electronic
Are you the author of this Elsevier article?	No
Will you be translating?	No
Title of new work	Modeling the Formation of the Hemozoin Crystal in the Presence of Antimalarials: A Theoretical Study
Institution name	University of Antioquia
Expected presentation date	Feb 2024
Portions	Fig 1 and Fig 2
Requestor Location	Universidad de AntioquiA Medellin, Colombia medellin, 055421 Colombia Attn: Universidad de AntioquiA
Publisher Tax ID	GB 494 6272 12
Total	0.00 USD
Terms and Conditions	

INTRODUCTION

1. The publisher for this copyrighted material is Elsevier. By clicking "accept" in connection with completing this licensing transaction, you agree that the following terms and conditions apply to this transaction (along with the Billing and Payment terms and conditions established by Copyright Clearance Center, Inc. ("CCC"), at the time that you opened your RightsLink account and that are available at any time at https://myaccount.copyright.com).

GENERAL TERMS

2. Elsevier hereby grants you permission to reproduce the aforementioned material subject to the terms and conditions indicated.

3. Acknowledgement: If any part of the material to be used (for example, figures) has appeared in our publication with credit or acknowledgement to another source, permission must also be sought from that source. If such permission is not obtained then that material may not be included in your publication/copies. Suitable acknowledgement to the source must be made, either as a footnote or in a reference list at the end of your publication, as follows:

"Reprinted from Publication title, Vol /edition number, Author(s), Title of article / title of chapter, Pages No., Copyright (Year), with permission from Elsevier [OR APPLICABLE SOCIETY COPYRIGHT OWNER]." Also Lancet special credit - "Reprinted from The Lancet, Vol. number, Author(s), Title of article, Pages No., Copyright (Year), with permission from Elsevier."

4. Reproduction of this material is confined to the purpose and/or media for which permission is hereby given. The material may not be reproduced or used in any other way, including use in combination with an artificial intelligence tool (including to train an algorithm, test, process, analyse, generate output and/or develop any form of artificial intelligence tool), or to create any derivative work and/or service (including resulting from the use of artificial intelligence tools).

5. Altering/Modifying Material: Not Permitted. However figures and illustrations may be altered/adapted minimally to serve your work. Any other abbreviations, additions, deletions and/or any other alterations shall be made only with prior written authorization of Elsevier Ltd. (Please contact Elsevier’s permissions helpdesk here). No modifications can be made to any Lancet figures/tables and they must be reproduced in full.

6. If the permission fee for the requested use of our material is waived in this instance, please be advised that your future requests for Elsevier materials may attract a fee.

7. Reservation of Rights: Publisher reserves all rights not specifically granted in the combination of (i) the license details provided by you and accepted in the course of this licensing transaction, (ii) these terms and conditions and (iii) CCC's Billing and Payment terms and conditions.

8. License Contingent Upon Payment: While you may exercise the rights licensed immediately upon issuance of the license at the end of the licensing process for the transaction, provided that you have disclosed complete and accurate details of your proposed use, no license is finally effective unless and until full payment is received from you (either by publisher or by CCC) as provided in CCC's Billing and Payment terms and conditions. If full payment is not received on a timely basis, then any license preliminarily granted shall be deemed automatically revoked and shall be void as if never granted. Further, in the event that you breach any of these terms and conditions or any of CCC's Billing and Payment terms and conditions, the license is automatically revoked and

shall be void as if never granted. Use of materials as described in a revoked license, as well as any use of the materials beyond the scope of an unrevoked license, may constitute copyright infringement and publisher reserves the right to take any and all action to protect its copyright in the materials.

9. Warranties: Publisher makes no representations or warranties with respect to the licensed material.

10. Indemnity: You hereby indemnify and agree to hold harmless publisher and CCC, and their respective officers, directors, employees and agents, from and against any and all claims arising out of your use of the licensed material other than as specifically authorized pursuant to this license.

11. No Transfer of License: This license is personal to you and may not be sublicensed, assigned, or transferred by you to any other person without publisher's written permission.

12. No Amendment Except in Writing: This license may not be amended except in a writing signed by both parties (or, in the case of publisher, by CCC on publisher's behalf).

13. Objection to Contrary Terms: Publisher hereby objects to any terms contained in any purchase order, acknowledgment, check endorsement or other writing prepared by you, which terms are inconsistent with these terms and conditions or CCC's Billing and Payment terms and conditions. These terms and conditions, together with CCC's Billing and Payment terms and conditions (which are incorporated herein), comprise the entire agreement between you and publisher (and CCC) concerning this licensing transaction. In the event of any conflict between your obligations established by these terms and conditions and those established by CCC's Billing and Payment terms and conditions, these terms and conditions shall control.

14. Revocation: Elsevier or Copyright Clearance Center may deny the permissions described in this License at their sole discretion, for any reason or no reason, with a full refund payable to you. Notice of such denial will be made using the contact information provided by you. Failure to receive such notice will not alter or invalidate the denial. In no event will Elsevier or Copyright Clearance Center be responsible or liable for any costs, expenses or damage incurred by you as a result of a denial of your permission request, other than a refund of the amount(s) paid by you to Elsevier and/or Copyright Clearance Center for denied permissions.

LIMITED LICENSE

The following terms and conditions apply only to specific license types:

15. **Translation**: This permission is granted for non-exclusive world **English** rights only unless your license was granted for translation rights. If you licensed translation rights you may only translate this content into the languages you requested. A professional translator must perform all translations and reproduce the content word for word preserving the integrity of the article.

16. **Posting licensed content on any Website**: The following terms and conditions apply as follows: Licensing material from an Elsevier journal: All content posted to the web site must maintain the copyright information line on the bottom of each image; A hyper-text must be included to the Homepage of the journal from which you are licensing at http://www.sciencedirect.com/science/journal/xxxxx or the Elsevier homepage for books at http://www.elsevier.com; Central Storage: This license does not include permission for

a scanned version of the material to be stored in a central repository such as that provided by Heron/XanEdu.

Licensing material from an Elsevier book: A hyper-text link must be included to the Elsevier homepage at http://www.elsevier.com . All content posted to the web site must maintain the copyright information line on the bottom of each image.

Posting licensed content on Electronic reserve: In addition to the above the following clauses are applicable: The web site must be password-protected and made available only to bona fide students registered on a relevant course. This permission is granted for 1 year only. You may obtain a new license for future website posting.

17. **For journal authors:** the following clauses are applicable in addition to the above:

Preprints:

A preprint is an author's own write-up of research results and analysis, it has not been peer-reviewed, nor has it had any other value added to it by a publisher (such as formatting, copyright, technical enhancement etc.).

Authors can share their preprints anywhere at any time. Preprints should not be added to or enhanced in any way in order to appear more like, or to substitute for, the final versions of articles however authors can update their preprints on arXiv or RePEc with their Accepted Author Manuscript (see below).

If accepted for publication, we encourage authors to link from the preprint to their formal publication via its DOI. Millions of researchers have access to the formal publications on ScienceDirect, and so links will help users to find, access, cite and use the best available version. Please note that Cell Press, The Lancet and some society-owned have different preprint policies. Information on these policies is available on the journal homepage.

Accepted Author Manuscripts: An accepted author manuscript is the manuscript of an article that has been accepted for publication and which typically includes author-incorporated changes suggested during submission, peer review and editor-author communications.

Authors can share their accepted author manuscript:

- immediately
  - via their non-commercial person homepage or blog
  - by updating a preprint in arXiv or RePEc with the accepted manuscript
  - via their research institute or institutional repository for internal institutional uses or as part of an invitation-only research collaboration work-group
  - directly by providing copies to their students or to research collaborators for their personal use
  - for private scholarly sharing as part of an invitation-only work group on commercial sites with which Elsevier has an agreement
- After the embargo period
  - via non-commercial hosting platforms such as their institutional repository
  - via commercial sites with which Elsevier has an agreement

In all cases accepted manuscripts should:

- link to the formal publication via its DOI

- bear a CC-BY-NC-ND license - this is easy to do
- if aggregated with other manuscripts, for example in a repository or other site, be shared in alignment with our hosting policy not be added to or enhanced in any way to appear more like, or to substitute for, the published journal article.

Published journal article (JPA): A published journal article (PJA) is the definitive final record of published research that appears or will appear in the journal and embodies all value-adding publishing activities including peer review co-ordination, copy-editing, formatting, (if relevant) pagination and online enrichment.

Policies for sharing publishing journal articles differ for subscription and gold open access articles:

Subscription Articles: If you are an author, please share a link to your article rather than the full-text. Millions of researchers have access to the formal publications on ScienceDirect, and so links will help your users to find, access, cite, and use the best available version.

Theses and dissertations which contain embedded PJAs as part of the formal submission can be posted publicly by the awarding institution with DOI links back to the formal publications on ScienceDirect.

If you are affiliated with a library that subscribes to ScienceDirect you have additional private sharing rights for others' research accessed under that agreement. This includes use for classroom teaching and internal training at the institution (including use in course packs and courseware programs), and inclusion of the article for grant funding purposes.

Gold Open Access Articles: May be shared according to the author-selected end-user license and should contain a CrossMark logo, the end user license, and a DOI link to the formal publication on ScienceDirect.

Please refer to Elsevier's posting policy for further information.

18. **For book authors** the following clauses are applicable in addition to the above: Authors are permitted to place a brief summary of their work online only. You are not allowed to download and post the published electronic version of your chapter, nor may you scan the printed edition to create an electronic version. **Posting to a repository:** Authors are permitted to post a summary of their chapter only in their institution's repository.

19. **Thesis/Dissertation**: If your license is for use in a thesis/dissertation your thesis may be submitted to your institution in either print or electronic form. Should your thesis be published commercially, please reapply for permission. These requirements include permission for the Library and Archives of Canada to supply single copies, on demand, of the complete thesis and include permission for Proquest/UMI to supply single copies, on demand, of the complete thesis. Should your thesis be published commercially, please reapply for permission. Theses and dissertations which contain embedded PJAs as part of the formal submission can be posted publicly by the awarding institution with DOI links back to the formal publications on ScienceDirect.

Elsevier Open Access Terms and Conditions

You can publish open access with Elsevier in hundreds of open access journals or in nearly 2000 established subscription journals that support open access publishing. Permitted third party re-use of these open access articles is defined by the author's choice of Creative Commons user license. See our open access license policy for more information.

Terms & Conditions applicable to all Open Access articles published with Elsevier:

Any reuse of the article must not represent the author as endorsing the adaptation of the article nor should the article be modified in such a way as to damage the author's honour or reputation. If any changes have been made, such changes must be clearly indicated.

The author(s) must be appropriately credited and we ask that you include the end user license and a DOI link to the formal publication on ScienceDirect.

If any part of the material to be used (for example, figures) has appeared in our publication with credit or acknowledgement to another source it is the responsibility of the user to ensure their reuse complies with the terms and conditions determined by the rights holder.

Additional Terms & Conditions applicable to each Creative Commons user license:

CC BY: The CC-BY license allows users to copy, to create extracts, abstracts and new works from the Article, to alter and revise the Article and to make commercial use of the Article (including reuse and/or resale of the Article by commercial entities), provided the user gives appropriate credit (with a link to the formal publication through the relevant DOI), provides a link to the license, indicates if changes were made and the licensor is not represented as endorsing the use made of the work. The full details of the license are available at http://creativecommons.org/licenses/by/4.0.

CC BY NC SA: The CC BY-NC-SA license allows users to copy, to create extracts, abstracts and new works from the Article, to alter and revise the Article, provided this is not done for commercial purposes, and that the user gives appropriate credit (with a link to the formal publication through the relevant DOI), provides a link to the license, indicates if changes were made and the licensor is not represented as endorsing the use made of the work. Further, any new works must be made available on the same conditions. The full details of the license are available at http://creativecommons.org/licenses/by-nc-sa/4.0.

CC BY NC ND: The CC BY-NC-ND license allows users to copy and distribute the Article, provided this is not done for commercial purposes and further does not permit distribution of the Article if it is changed or edited in any way, and provided the user gives appropriate credit (with a link to the formal publication through the relevant DOI), provides a link to the license, and that the licensor is not represented as endorsing the use made of the work. The full details of the license are available at http://creativecommons.org/licenses/by-nc-nd/4.0. Any commercial reuse of Open Access articles published with a CC BY NC SA or CC BY NC ND license requires permission from Elsevier and will be subject to a fee.

Commercial reuse includes:

- Associating advertising with the full text of the Article
- Charging fees for document delivery or access
- Article aggregation
- Systematic distribution via e-mail lists or share buttons

Posting or linking by commercial companies for use by customers of those companies.

20. **Other Conditions**:

v1.10

Questions? customercare@copyright.com.

References

[1] Robert F Pasternack, Ben Munda, Abigail Bickford, Esther J Gibbs, and Luigi Monsù Scolaro. On the kinetics of formation of hemozoin, the malaria pigment. *Journal of inorganic biochemistry*, 104(10):1119–1124, 2010.

[2] Julieth Herrera, Cristian Parra, Daniel Coronado Cardona, Valentina Perez, Julian Zapata, Adriana Pabón, Olga Lopez-Acevedo, Karen García, and César Barrero Meneses. Revising the formation of β-hematin crystals from hemin in aqueous-acetate medium containing chloroquine: Modeling the kinetics of crystallization and characterizing their physicochemical properties. *Crystal Growth & Design*, 2023.

[3] Ask Hjorth Larsen, Jens Jørgen Mortensen, Jakob Blomqvist, Ivano E Castelli, Rune Christensen, Marcin Dułak, Jesper Friis, Michael N Groves, Bjørk Hammer, Cory Hargus, et al. The atomic simulation environment—a python library for working with atoms. *Journal of Physics: Condensed Matter*, 29(27):273002, 2017.

[4] Jens Jørgen Mortensen, Lars Bruno Hansen, and Karsten Wedel Jacobsen. Real-space grid implementation of the projector augmented wave method. *Physical review B*, 71(3):035109, 2005.

[5] David Sullivan and Sanjeev Krishna. *Malaria: drugs, disease and post-genomic biology*, volume 295. Springer Science & Business Media, 2006.

[6] World Health Organization et al. *World malaria report 2022*. World Health Organization, 2022.

[7] Richard Lucius, Brigitte Loos-Frank, Richard P Lane, Robert Poulin, Craig Roberts, and Richard K Grencis. *The biology of parasites*. John Wiley & Sons, 2017.

[8] Louis H Miller and Xinzhuan Su. Artemisinin: discovery from the chinese herbal garden. *Cell*, 146(6):855–858, 2011.

[9] Charles J Woodrow and Nicholas J White. The clinical impact of artemisinin resistance in southeast asia and the potential for future spread. *FEMS microbiology reviews*, 41(1):34–48, 2017.

[10] Gabriel Gachelin, Paul Garner, Eliana Ferroni, Ulrich Tröhler, and Iain Chalmers. Evaluating cinchona bark and quinine for treating and preventing malaria. *Journal of the Royal Society of Medicine*, 110(1):31–40, 2017.

[11] Lewis Tanenbaum and Denny L Tuffanelli. Antimalarial agents: chloroquine, hydroxychloroquine, and quinacrine. *Archives of dermatology*, 116(5):587–591, 1980.

[12] Thomas E Wellems and Christopher V Plowe. Chloroquine-resistant malaria. *The Journal of infectious diseases*, 184(6):770–776, 2001.

[13] U D'alessandro and H Buttiens. History and importance of antimalarial drug resistance. *Tropical Medicine & International Health*, 6(11):845–848, 2001.

[14] Andrew FG Slater. Chloroquine: mechanism of drug action and resistance in plasmodium falciparum. *Pharmacology & therapeutics*, 57(2-3):203–235, 1993.

[15] Kim Y Fong and David W Wright. Hemozoin and antimalarial drug discovery. *Future medicinal chemistry*, 5(12):1437–1450, 2013.

[16] John M Pisciotta and David Sullivan. Hemozoin: oil versus water. *Parasitology international*, 57(2):89–96, 2008.

[17] Sergey Kapishnikov, Daniel Grolimund, Gerd Schneider, Eva Pereiro, James G McNally, Jens Als-Nielsen, and Leslie Leiserowitz. Unraveling heme detoxification in the malaria parasite by in situ correlative x-ray fluorescence microscopy and soft x-ray tomography. *Scientific Reports*, 7(1):7610, 2017.

[18] Sahil Kumar, TR Bhardwaj, DN Prasad, and Rajesh K Singh. Drug targets for resistant malaria: historic to future perspectives. *Biomedicine & Pharmacotherapy*, 104:8–27, 2018.

[19] Johandie Gildenhuys, Tanya le Roex, Timothy J Egan, and Katherine A de Villiers. The single crystal x-ray structure of β-hematin dmso solvate grown in the presence of chloroquine, a β-hematin growth-rate inhibitor. *Journal of the American Chemical Society*, 135(3):1037–1047, 2013.

[20] Nectarios Klonis, Ruben Dilanian, Eric Hanssen, Connie Darmanin, Victor Streltsov, Samantha Deed, Harry Quiney, and Leann Tilley. Hematin- hematin self-association states involved in the formation and reactivity of the malaria parasite pigment, hemozoin. *Biochemistry*, 49(31):6804–6811, 2010.

[21] Noa Marom, Alexandre Tkatchenko, Sergey Kapishnikov, Leeor Kronik, and Leslie Leiserowitz. Structure and formation of synthetic hemozoin: insights from first-principles calculations. *Crystal growth & design*, 11(8):3332–3341, 2011.

[22] Katherine A de Villiers and Timothy J Egan. Heme detoxification in the malaria parasite: A target for antimalarial drug development. *Accounts of chemical research*, 54(11):2649–2659, 2021.

[23] Lorena M Coronado, Christopher T Nadovich, and Carmenza Spadafora. Malarial hemozoin: from target to tool. *Biochimica et Biophysica Acta (BBA)-General Subjects*, 1840(6):2032–2041, 2014.

[24] Katy N Olafson, Megan A Ketchum, Jeffrey D Rimer, and Peter G Vekilov. Mechanisms of hematin crystallization and inhibition by the antimalarial drug chloroquine. *Proceedings of the National Academy of Sciences*, 112(16):4946–4951, 2015.

[25] Omar Rifaie-Graham, Xiao Hua, Nico Bruns, and Sandor Balog. The kinetics of β-hematin crystallization measured by depolarized light scattering. *Small*, 14(46):1802295, 2018.

[26] James J De Yoreo and Peter G Vekilov. Principles of crystal nucleation and growth. *Reviews in mineralogy and geochemistry*, 54(1):57–93, 2003.

[27] Camila Wendt, Wanderley de Souza, Alessandro Pinheiro, Leandro Silva, Ana Acacia de Sa Pinheiro, Raynald Gauvin, and Kildare Miranda. High-resolution electron microscopy analysis of malaria hemozoin crystals reveals new aspects of crystal growth and elemental composition. *Crystal Growth & Design*, 21(10):5521–5533, 2021.

[28] Silvina Pagola, Peter W Stephens, D Scott Bohle, Andrew D Kosar, and Sara K Madsen. The structure of malaria pigment β-haematin. *Nature*, 404(6775):307–310, 2000.

[29] Katherine A de Villiers, Catherine H Kaschula, Timothy J Egan, and Helder M Marques. Speciation and structure of ferriprotoporphyrin ix in aqueous solution: spectroscopic and diffusion measurements demonstrate dimerization, but not μ-oxo dimer formation. *JBIC Journal of Biological Inorganic Chemistry*, 12:101–117, 2007.

[30] Dirk Porezag and Mark R Pederson. Infrared intensities and raman-scattering activities within density-functional theory. *Physical Review B*, 54(11):7830, 1996.

[31] Bayden R Wood, Steven J Langford, Brian M Cooke, Janelle Lim, Fiona K Glenister, Martin Duriska, Jessica K Unthank, and Don McNaughton. Resonance raman spectroscopy reveals new insight into the electronic structure of β-hematin and malaria pigment. *Journal of the American Chemical Society*, 126(30):9233–9239, 2004.

[32] Md Ehesan Ali and Peter M Oppeneer. Unraveling the electronic structure, spin states, optical and vibrational spectra of malaria pigment. *Chemistry–A European Journal*, 21(23):8544–8553, 2015.

[33] Gérard Y Vichniac. Simulating physics with cellular automata. *Physica D: Nonlinear Phenomena*, 10(1-2):96–116, 1984.

[34] James E House. *Principles of chemical kinetics*. Academic press, 2007.

[35] Ernő Keszei. *Reaction Kinetics: An Introduction*. Springer Nature, 2021.

[36] S Karthika, TK Radhakrishnan, and P Kalaichelvi. A review of classical and nonclassical nucleation theories. *Crystal Growth & Design*, 16(11):6663–6681, 2016.

[37] Sanjay Puri. Kinetics of phase transitions. In *Kinetics of phase transitions*, pages 13–74. CRC press, 2009.

[38] Sergey Kapishnikov, Ernst Hempelmann, Michael Elbaum, Jens Als-Nielsen, and Leslie Leiserowitz. Malaria pigment crystals: The achilles′ heel of the malaria parasite. *ChemMedChem*, 16(10):1515–1532, 2021.

[39] Sergey Kapishnikov, Allon Weiner, Eyal Shimoni, Gerd Schneider, Michael Elbaum, and Leslie Leiserowitz. Digestive vacuole membrane in plasmodium falciparum-infected erythrocytes: Relevance to templated nucleation of hemozoin. *Langmuir*, 29(47):14595–14602, 2013.

[40] Deniz Erdemir, Alfred Y Lee, and Allan S Myerson. Nucleation of crystals from solution: classical and two-step models. *Accounts of chemical research*, 42(5):621–629, 2009.

[41] Jianmin Zhou, Yixin Zhou, and Weiwei Tang. Molecular mechanism of organic crystal nucleation: A perspective of solution chemistry and polymorphism. *Crystals*, 12(7):980, 2022.

[42] Alejandro G Marangoni and Alejandro G Marangoni. Kinetics of crystal growth using the avrami model and the chemical potential approach. *Kinetic analysis of food systems*, pages 113–134, 2017.

[43] Kiana Shirzad and Christopher Viney. A critical review on applications of the avrami equation beyond materials science. *Journal of the Royal Society Interface*, 20(203):20230242, 2023.

[44] Timothy J Egan, Winile W Mavuso, and Kanyile K Ncokazi. The mechanism of β-hematin formation in acetate solution. parallels between hemozoin formation and biomineralization processes. *Biochemistry*, 40(1):204–213, 2001.

[45] Renata Stiebler, Anh N Hoang, Timothy J Egan, David W Wright, and Marcus F Oliveira. Increase on the initial soluble heme levels in acidic conditions is an important mechanism for spontaneous heme crystallization in vitro. *PLoS One*, 5(9):e12694, 2010.

[46] Sharné-Maré Fitzroy, Johandie Gildenhuys, Tania Olivier, Ndivhuwo Olga Tshililo, David Kuter, and Katherine Allison de Villiers. The effects of quinoline and non-quinoline inhibitors on the kinetics of lipid-mediated β-hematin crystallization. *Langmuir*, 33(30):7529–7537, 2017.

[47] Inna Solomonov, Maria Osipova, Yishay Feldman, Carsten Baehtz, Kristian Kjaer, Ian K Robinson, Grant T Webster, Don McNaughton, Bayden R Wood, Isabelle Weissbuch, et al. Crystal nucleation, growth, and morphology of the synthetic malaria pigment β-hematin and the effect thereon by quinoline additives: the malaria pigment as a target of various antimalarial drugs. *Journal of the American Chemical Society*, 129(9):2615–2627, 2007.

[48] Anh N Hoang, Kanyile K Ncokazi, Katherine A de Villiers, David W Wright, and Timothy J Egan. Crystallization of synthetic haemozoin (β-haematin) nucleated at the surface of lipid particles. *Dalton Transactions*, 39(5):1235–1244, 2010.

[49] Andrew R Conn, Nicholas IM Gould, and Philippe L Toint. *Trust region methods*. SIAM, 2000.

[50] Liwang Cui and Xin-zhuan Su. Discovery, mechanisms of action and combination therapy of artemisinin. *Expert review of anti-infective therapy*, 7(8):999–1013, 2009.

[51] Juan I Rodriguez, Fernando Cortés-Guzmán, and James SM Anderson. *Advances in Quantum Chemical Topology Beyond QTAIM*. Elsevier, 2022.

[52] Klaus Capelle. A bird's-eye view of density-functional theory. *Brazilian journal of physics*, 36:1318–1343, 2006.

[53] Tanja Van Mourik, Michael Bühl, and Marie-Pierre Gaigeot. Density functional theory across chemistry, physics and biology, 2014.

[54] Jussi Enkovaara, Carsten Rostgaard, J Jørgen Mortensen, Jingzhe Chen, M Dułak, Lara Ferrighi, Jeppe Gavnholt, Christian Glinsvad, V Haikola, HA Hansen, et al. Electronic structure calculations with gpaw: a real-space implementation of the projector augmented-wave method. *Journal of physics: Condensed matter*, 22(25):253202, 2010.

[55] John P Perdew, Kieron Burke, and Matthias Ernzerhof. Generalized gradient approximation made simple. *Physical review letters*, 77(18):3865, 1996.

[56] Alexandre Tkatchenko and Matthias Scheffler. Accurate molecular van der waals interactions from ground-state electron density and free-atom reference data. *Physical review letters*, 102(7):073005, 2009.

[57] Barbara H Stuart. *Infrared spectroscopy: fundamentals and applications*. John Wiley & Sons, 2004.

[58] Xiao-Yan Liu, Ya-Ning Xu, Hao-Cheng Wang, Jing-Wen Cao, Xiao-Ling Qin, and Peng Zhang. First-principles dft investigations of the vibrational spectra of chloroquine and hydroxychloroquine. *Journal of Physics Communications*, 5(10):105009, 2021.

[59] Maria P Crespo, Leann Tilley, and Nectarios Klonis. Solution behavior of hematin under acidic conditions and implications for its interactions with chloroquine. *JBIC Journal of Biological Inorganic Chemistry*, 15:1009–1022, 2010.

[60] RL Goetz. Particle stimulated nucleation during dynamic recrystallization using a cellular automata model. *Scripta Materialia*, 52(9):851–856, 2005.

[61] Marianne Delorme and Jacques Mazoyer. *Cellular automata: A parallel model*, volume 460. Springer Science & Business Media, 1998.

[62] Martin Gardner. The fantastic combinations of jhon conway's new solitaire game'life. *Sc. Am.*, 223:20–123, 1970.

[63] Sukanta Das, Souvik Roy, and Kamalika Bhattacharjee. *The Mathematical Artist: A Tribute To John Horton Conway*, volume 45. Springer Nature, 2022.

[64] Katarina E Blow, David Quigley, and Gabriele C Sosso. The seven deadly sins: When computing crystal nucleation rates, the devil is in the details. *The Journal of Chemical Physics*, 155(4), 2021.

[65] D Scott Bohle, Erin L Dodd, and Peter W Stephens. Structure of malaria pigment and related propanoate-linked metalloporphyrin dimers. *Chemistry & Biodiversity*, 9(9):1891–1902, 2012.